

Classical three rotor problem: Periodic solutions, stability and chaos

Cite as: Chaos **29**, 123121 (2019); <https://doi.org/10.1063/1.5110032>

Submitted: 14 May 2019 . Accepted: 02 December 2019 . Published Online: 17 December 2019

Govind S. Krishnaswami , and Himalaya Senapati 

COLLECTIONS

 This paper was selected as an Editor's Pick



View Online



Export Citation



CrossMark

ARTICLES YOU MAY BE INTERESTED IN

[Dynamical equivalence between Kuramoto models with first- and higher-order coupling](#)

Chaos: An Interdisciplinary Journal of Nonlinear Science **29**, 113129 (2019); <https://doi.org/10.1063/1.5118941>

[On the intersection of a chaotic attractor and a chaotic repeller in the system of two adaptively coupled phase oscillators](#)

Chaos: An Interdisciplinary Journal of Nonlinear Science **29**, 111102 (2019); <https://doi.org/10.1063/1.5130994>

[Mixed global dynamics of forced vibro-impact oscillator with Coulomb friction](#)

Chaos: An Interdisciplinary Journal of Nonlinear Science **29**, 113116 (2019); <https://doi.org/10.1063/1.5095627>

AIP Conference Proceedings
FLASH WINTER SALE!

50% OFF ALL PRINT PROCEEDINGS

ENTER CODE 50DEC19 AT CHECKOUT



Classical three rotor problem: Periodic solutions, stability and chaos

Cite as: Chaos 29, 123121 (2019); doi: 10.1063/1.5110032

Submitted: 14 May 2019 · Accepted: 2 December 2019 ·

Published Online: 17 December 2019



View Online



Export Citation



CrossMark

Govind S. Krishnaswami^{a)}  and Himalaya Senapati^{b)} 

AFFILIATIONS

Physics Department, Chennai Mathematical Institute, SIPCOT IT Park, Siruseri, Chennai 603103, India

^{a)}Electronic mail: govind@cmi.ac.in. URL: <https://www.cmi.ac.in/~govind/>

^{b)}Electronic mail: himalay@cmi.ac.in

ABSTRACT

This paper concerns the classical dynamics of three coupled rotors: equal masses moving on a circle subject to attractive cosine interparticle potentials. This system arises as the classical limit of a model of coupled Josephson junctions. In appropriate units, the non-negative energy E of the relative motion is the only free parameter. We find families of periodic solutions: pendulum and isosceles solutions at all energies and choreographies up to moderate energies. The model displays order-chaos-order behavior: it is integrable at zero and infinitely high energies but displays a fairly sharp transition from regular to chaotic behavior as E is increased beyond $E_c \approx 4$ and a more gradual return to regularity. The transition to chaos is manifested in a dramatic rise of the fraction of the area of the Hill region of Poincaré surfaces occupied by chaotic sections and also in the spontaneous breaking of discrete symmetries of Poincaré sections present at lower energies. Interestingly, the above pendulum solutions alternate between being stable and unstable, with the transition energies cascading geometrically from either sides at $E = 4$. The transition to chaos is also reflected in the curvature of the Jacobi-Maupertuis metric that ceases to be everywhere positive when E exceeds four. Examination of Poincaré sections also indicates global chaos in a band of energies ($5.33 \lesssim E \lesssim 5.6$) slightly above this transition.

Published under license by AIP Publishing. <https://doi.org/10.1063/1.5110032>

We study the classical dynamics of three equal point masses moving on a circle subject to attractive cosine interparticle potentials. This three-rotor problem, where rotors can pass through each other, arises as the classical limit of a chain of coupled Josephson junctions. In center of mass variables, the relative energy E serves as a control parameter. We discover three classes of periodic solutions: choreographies up to moderate energies and pendula and breathers at all energies. The system is integrable at zero and infinite energies but displays a fairly sharp transition to chaos around $E \approx 4$, thus providing an instance of the order-chaos-order transition. We find several manifestations of this transition: (a) a geometric cascade of stable to unstable transition energies in pendula as $E \rightarrow 4^\pm$; (b) a transition in the curvature of the Jacobi-Maupertuis metric from being positive to having both signs as E exceeds four, implying widespread onset of instabilities; (c) a dramatic rise in the fraction of the area of Poincaré surfaces occupied by chaotic trajectories and (d) a breakdown of discrete symmetries in Poincaré sections present at lower energies. Slightly above this transition, we find evidence for a band of global chaos where we conjecture ergodic behavior.

I. INTRODUCTION

We study the problem of three rotors, where three particles of equal mass m move on a circle subject to attractive cosine interparticle potentials of strength g . The rotors can pass through each other so that there are no collisions. While the problem of two rotors reduces to that of a simple pendulum, the dynamics of three (or more) rotors is rich and displays novel signatures of the transition to chaos as the coupling g (or energy) is varied.

The quantum n -rotor problem is also of interest as it is used to model a chain of coupled Josephson junctions.¹ Here, the rotor angles are the phases of the superconducting order parameters associated with the segments between junctions. While in the application to the insulator-to-superconductor transition in arrays of Josephson junctions, one is typically interested in the limit of large n , here we focus on the classical dynamics of the $n = 3$ case.

In Sec. II, we begin by formulating the classical three-rotor problem and eliminate the center of mass motion to arrive at dynamics on a 2-dimensional configuration torus parametrized by the relative angles φ_1 and φ_2 . In Sec. III, we discuss the dynamics on the φ_1 - φ_2 torus, find all static solutions for the relative motion, and

discuss their stability (see Fig. 1). The system is also shown to be integrable at zero and infinitely high relative energies E (compared to the coupling g) due to the emergence of additional conserved quantities. Furthermore, we also describe changes in the topology of the Hill region of the configuration space at $E = 0, 4g$, and $4.5g$ (see Fig. 2).

In Sec. IV, we use consistent reductions of the equations of motion to one degree of freedom to find pendulum and isosceles families of periodic solutions at all energies (see Fig. 3). We investigate the stability of the pendula and breathers by computing their monodromies. Notably, we find that the stability index of pendula becomes periodic on a log scale as $E \rightarrow 4g^\pm$ and shows an accumulation of stable to unstable transition energies at $E = 4g$ (see Fig. 4). In other words, the largest Lyapunov exponent switches from positive to zero infinitely often with the widths of the (un)stable windows asymptotically approaching a geometric sequence as $E \rightarrow 4g^\pm$.

In Sec. V, we reformulate the dynamics on the φ_1 - φ_2 torus as geodesic flow with respect to the Jacobi-Maupertuis metric. We prove in Appendix A that the scalar curvature is strictly positive on the Hill region for $0 \leq E \leq 4g$ but acquires both signs above $E = 4g$ (Fig. 7) indicating the onset of widespread geodesic instabilities. In Sec. VI, we examine Poincaré sections and observe a marked transition to chaos in the neighborhood of $E = 4g$ as manifested in a rapid rise of the fraction of the area of the energetically allowed “Hill” region occupied by chaotic sections (Fig. 12). This is accompanied by a spontaneous breaking of two discrete symmetries of low energy Poincaré sections (Figs. 9 and 10). This transition also coincides with the accumulation of stable to unstable transition energies of the pendulum family of periodic solutions at $E = 4g$. Slightly above this energy, we find a band of global chaos $5.33g \lesssim E \lesssim 5.6g$, where the chaotic sections fill up the entire Hill region on all Poincaré surfaces, suggesting ergodic behavior (see Fig. 13). In Sec. VII, we derive a system of delay differential and algebraic equations for periodic choreography solutions of the three-rotor problem. We discover three families of choreographies. The first pair are uniformly rotating versions of two of the static solutions for the relative motion. The third family is nonrotating, stable, and exists for all relative energies up to the onset of global chaos (see Fig. 14). It is found by a careful examination of Poincaré sections. Finally, we prove that choreographies cannot exist for arbitrarily high relative energies. We conclude with a discussion in Sec. VIII. Appendix B summarizes the numerical method employed to estimate the fraction of chaos on Poincaré surfaces. A preliminary version of this paper was presented at the Conference on Nonlinear Systems and Dynamics, New Delhi, October 2018.²

II. THREE COUPLED CLASSICAL ROTORS

We study a periodic chain of three identical rotors of mass m interacting via cosine potentials. The Lagrangian is

$$L = \sum_{i=1}^3 \left\{ \frac{1}{2} mr^2 \dot{\theta}_i^2 - g[1 - \cos(\theta_i - \theta_{i+1})] \right\} \quad (1)$$

with $\theta_4 \equiv \theta_1$. Here, θ_i are 2π -periodic coordinates on a circle of radius r . Though we only have nearest neighbor interactions, each pair interacts as there are only three rotors. We consider “ferromagnetic” coupling $g > 0$ so that the rotors attract each other. Unlike with

gravity, the inter-rotor forces vanish when rotors coincide so that they can “pass” through each other: this is physically apt since they occupy distinct sites. The equations of motion for $i = 1, 2$, and 3 are

$$mr^2 \ddot{\theta}_i = g \sin(\theta_{i-1} - \theta_i) - g \sin(\theta_i - \theta_{i+1}) \quad (2)$$

with $\theta_{0,1} \equiv \theta_{3,4}$. The configuration space is a 3-torus $0 \leq \theta_i \leq 2\pi$ with conjugate angular momenta $\pi_i = mr^2 \dot{\theta}_i$ and

$$H = \sum_{i=1}^3 \left\{ \frac{\pi_i^2}{2mr^2} + g[1 - \cos(\theta_i - \theta_{i+1})] \right\}. \quad (3)$$

Hamilton’s equations,

$$mr^2 \dot{\theta}_i = \pi_i \quad \text{and} \quad \dot{\pi}_i = g[\sin(\theta_{i-1} - \theta_i) - \sin(\theta_i - \theta_{i+1})], \quad (4)$$

define a smooth Hamiltonian vector field on the 6d phase space. The additive constant in H is chosen so that its minimal value is zero. This system has 3 independent dimensionful physical parameters m , r , and g that can be put to one by a choice of units. However, once such a choice of units has been made, all other physical quantities (like \hbar) have definite numerical values. This circumstance is similar to that in the Toda model.³

In Sec. V, we will reformulate the dynamics as geodesic flow on T^2 (or T^3 upon including center of mass motion, see below), which is geodesically complete. For $E > 4.5g$, this is expected on account of compactness and lack of boundary of the energetically allowed Hill region. For $E < 4.5g$, though the trajectories can (in finite time) reach the Hill boundary, they simply turn around. Examples of such trajectories are provided by the $\varphi_1 = 0$ pendulum solutions described in Sec. IV A.

Center of Mass (CM) and relative coordinates: It is convenient to define the CM and relative angles

$$\varphi_0 = (\theta_1 + \theta_2 + \theta_3)/3, \quad \varphi_1 = \theta_1 - \theta_2, \quad \text{and} \quad \varphi_2 = \theta_2 - \theta_3. \quad (5)$$

As a consequence of the 2π -periodicity of θ s, φ_0 is 2π -periodic, while $\varphi_{1,2}$ is 6π -periodic. However, the cuboid ($0 \leq \varphi_0 \leq 2\pi$, $0 \leq \varphi_{1,2} \leq 6\pi$) is a ninefold cover of the fundamental cuboid $0 \leq \theta_{1,2,3} \leq 2\pi$. In fact, since the configurations $(\varphi_0, \varphi_1 - 2\pi, \varphi_2)$, $(\varphi_0, \varphi_1, \varphi_2 + 2\pi)$, and $(\varphi_0 + 2\pi/3, \varphi_1, \varphi_2)$ are physically identical, we may restrict $\varphi_{1,2}$ to lie in $[0, 2\pi]$. Here, φ_i are not quite periodic coordinates on $T^3 \equiv [0, 2\pi]^3$. Rather, when $\varphi_1 \mapsto \varphi_1 \pm 2\pi$ or $\varphi_2 \mapsto \varphi_2 \mp 2\pi$, the CM variable $\varphi_0 \mapsto \varphi_0 \pm 2\pi/3$. In these coordinates, the Lagrangian becomes $L = T - V$, where

$$T = \frac{3}{2} mr^2 \dot{\varphi}_0^2 + \frac{1}{3} mr^2 [\dot{\varphi}_1^2 + \dot{\varphi}_2^2 + \dot{\varphi}_1 \dot{\varphi}_2] \quad \text{and}$$

$$V = g[3 - \cos \varphi_1 - \cos \varphi_2 - \cos(\varphi_1 + \varphi_2)], \quad (6)$$

with the equations of motion (EOM) $3mr^2 \ddot{\varphi}_0 = 0$,

$$mr^2 \ddot{\varphi}_1 = -g[2 \sin \varphi_1 - \sin \varphi_2 + \sin(\varphi_1 + \varphi_2)], \quad 1 \leftrightarrow 2. \quad (7)$$

The conjugate momenta are $p_0 = 3mr^2 \dot{\varphi}_0$,

$$p_1 = (mr^2/3)(2\dot{\varphi}_1 + \dot{\varphi}_2), \quad p_2 = (mr^2/3)(\dot{\varphi}_1 + 2\dot{\varphi}_2). \quad (8)$$

The EOM admit a conserved energy which is a sum of CM, relative kinetic and potential energies,

$$E = \frac{3}{2} mr^2 \dot{\varphi}_0^2 + \frac{1}{3} mr^2 [\dot{\varphi}_1^2 + \dot{\varphi}_2^2 + \dot{\varphi}_1 \dot{\varphi}_2] + V(\varphi_1, \varphi_2). \quad (9)$$

III. DYNAMICS ON THE φ_1 - φ_2 TORUS

The dynamics of φ_1 and φ_2 (or equivalently that of φ_{\pm}) decouples from that of the CM coordinate φ_0 . The former may be regarded as periodic coordinates on the 2-torus $[0, 2\pi] \times [0, 2\pi]$. On the other hand, φ_0 , which may be regarded as a fiber coordinate over the $\varphi_{1,2}$ base torus, evolves according to

$$\varphi_0 = \frac{p_0 t}{3mr^2} + \varphi_0(0) + \frac{2\pi}{3}(n_2 - n_1) \pmod{2\pi}. \quad (10)$$

Here, $n_{1,2}$ are the “greatest integer winding numbers” of the trajectory around the cycles of the base torus. If a trajectory goes continuously from $\varphi_{1,2}^i$ to $\varphi_{1,2}^f$ (regarded as real rather than modulo 2π), then the greatest integer winding numbers are defined as $n_{1,2} = [(\varphi_{1,2}^f - \varphi_{1,2}^i)/2\pi]$.

Consequently, we may restrict our attention to the dynamics of φ_1 and φ_2 . The equations of motion on the corresponding 4d phase space (the cotangent bundle of the 2-torus) are

$$\dot{\varphi}_1 = (2p_1 - p_2)/mr^2, \quad \dot{p}_1 = -g[\sin \varphi_1 + \sin(\varphi_1 + \varphi_2)], \quad (11)$$

and $1 \leftrightarrow 2$. These equations define a singularity-free vector field on the phase space. They follow from the canonical Poisson brackets (PBs) with Hamiltonian given by the relative energy

$$H_{\text{rel}} = \frac{p_1^2 + p_2^2 - p_1 p_2}{mr^2} + V(\varphi_1, \varphi_2). \quad (12)$$

Static solutions and their stability: Static solutions for the relative motion correspond to zeros of the vector field, where the force components in (11) vanish: $p_1 = p_2 = 0$ and

$$\sin \varphi_1 + \sin(\varphi_1 + \varphi_2) = \sin \varphi_2 + \sin(\varphi_1 + \varphi_2) = 0. \quad (13)$$

In particular, we must have $\varphi_1 = \varphi_2$ or $\varphi_1 = \pi - \varphi_2$. When $\varphi_1 = \varphi_2$, the force components are both equal to $\sin \varphi_1(1 + 2 \cos \varphi_1)$, which vanishes at the following configurations:

$$(\varphi_1, \varphi_2) = (0, 0), \quad (\pi, \pi), \quad \text{and} \quad (\pm 2\pi/3, \pm 2\pi/3). \quad (14)$$

On the other hand, if $\varphi_1 = \pi - \varphi_2$, we must have $\sin \varphi_1 = 0$ leading to two more static configurations $(0, \pi)$ and $(\pi, 0)$. Thus, we have six

static solutions which we list in increasing order of (relative) energy (see Fig. 1),

$$\begin{aligned} E = 0 : G(0, 0), \quad E = 4g : D_1(\pi, \pi), D_2(\pi, 0), D_3(0, \pi), \\ \text{and } E = 9g/2 : T_{1,2}(\pm 2\pi/3, \pm 2\pi/3). \end{aligned} \quad (15)$$

Uniformly rotating solutions from G, D, and T: If we include the uniform rotation of the CM angle ($\dot{\varphi}_0 = \Omega$ is arbitrary), these six solutions correspond to the following uniformly rotating rigid configurations of 3-rotors (see Fig. 1): (a) the ferromagnetic ground state G where the three particles coalesce ($\theta_1 = \theta_2 = \theta_3$), (b) the three “diagonal” “antiferromagnetic Néel” states D where two particles coincide and the third is diametrically opposite ($\theta_1 = \theta_2 = \theta_3 + \pi$ and cyclic permutations thereof), and (c) the two “triangle” “spin wave” states T where the three bodies are equally separated ($\theta_1 = \theta_2 + 2\pi/3 = \theta_3 + 4\pi/3$ and $\theta_2 \leftrightarrow \theta_3$).

Stability of static solutions: The linearized EOM (7) for perturbations to G, D, and T [$\varphi_{1,2} = \bar{\varphi}_{1,2} + \delta\varphi_{1,2}(t)$] are

$$\begin{aligned} mr^2 \frac{d^2}{dt^2} \begin{pmatrix} \delta\varphi_1 \\ \delta\varphi_2 \end{pmatrix} = -gA \begin{pmatrix} \delta\varphi_1 \\ \delta\varphi_2 \end{pmatrix} \quad \text{where } A_G = 3I, \\ A_{D_3(0,\pi)} = \begin{pmatrix} 1 & 0 \\ -2 & -3 \end{pmatrix}, \quad A_{D_2(\pi,0)} = \begin{pmatrix} -3 & -2 \\ 0 & 1 \end{pmatrix}, \quad (16) \\ A_{D_1(\pi,\pi)} = \begin{pmatrix} -1 & 2 \\ 2 & -1 \end{pmatrix} \quad \text{and} \quad A_T = -3I/2. \end{aligned}$$

Here, I is the 2×2 identity matrix. Perturbations to G are stable and lead to small oscillations with equal frequencies $\omega_0 = \sqrt{3g/mr^2}$. The saddles D have one stable direction with frequency $\omega_0/\sqrt{3}$ and one unstable eigendirection with growth rate ω_0 . On the other hand, both eigendirections around T are unstable with growth rate $\omega_0/\sqrt{2}$.

Changes in the topology of the Hill region with energy: The Hill region of possible motions \mathcal{H}_E at energy E is the subset $V(\varphi_1, \varphi_2) \leq E$ of the φ_1 - φ_2 configuration torus. The topology of the Hill region for various energies can be read-off from Fig. 1(a). For instance, for $0 < E < 4g$, \mathcal{H}_E is a disk while it is the whole torus for $E > 4.5g$. For $4g < E < 4.5g$, it has the topology of a torus with a

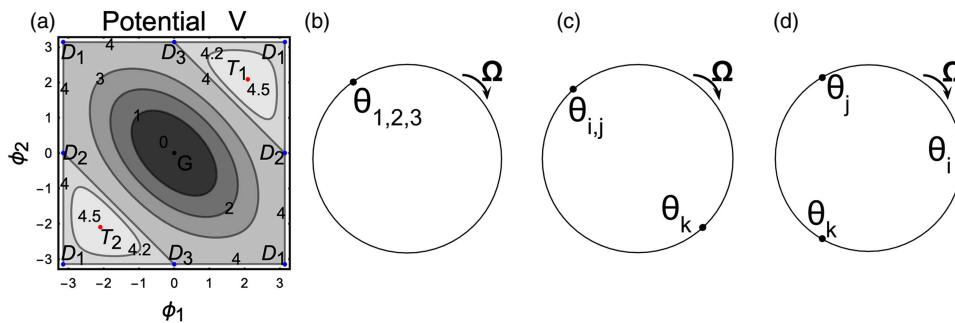


FIG. 1. (a) Potential energy V in units of g on the φ_1 - φ_2 configuration torus with its extrema (locations of static solutions G, D, and T) indicated. The contours also encode changes in the topology of the Hill region ($V \leq E$) when E crosses $E_G = 0$, $E_D = 4g$, and $E_T = 4.5g$. (b)–(d) Uniformly rotating three-rotor solutions obtained from G, D, and T. Here, i, j , and k denote any permutation of the numerals 1, 2 and 3. (b) and (d) are the simplest examples of choreographies discussed in Sec. VII. (a) Contours of V , (b) Ground state G. (c) Diagonal states D. (d) Triangle states T.

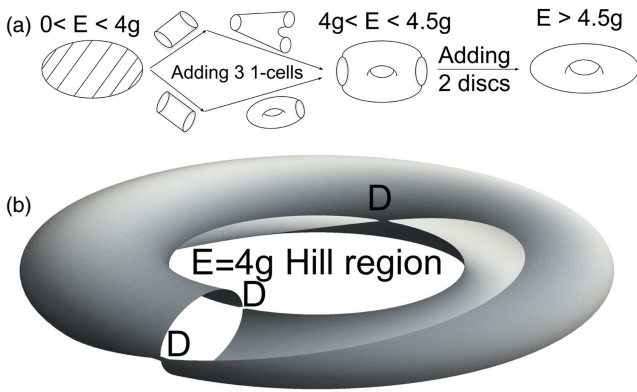


FIG. 2. (a) Topology of the Hill region of configuration space $V(\varphi_1, \varphi_2) \leq E$ showing transitions at $E = 4g$ and $4.5g$. (b) The Hill region for $E = 4g$ is not quite a manifold; its boundary consists of 3 noncontractible closed curves on the torus meeting at the static saddle configurations $D_{1,2,3}$.

pair of disks (around T_1 and T_2) excised. These changes in topology are confirmed by the Morse theory⁴ if we treat V as a real-valued Morse function, since its critical points are nondegenerate. In fact, the critical points of V are located at G (minimum with index 0), $D_{1,2,3}$ (saddles with indices 1), and $T_{1,2}$ (maxima with indices 2). Thus, the topology of \mathcal{H}_E can change only at the critical values $E_G = 0$, $E_D = 4g$, and $E_T = 4.5g$ [see Fig. 2(a)]. At $E = 0$, the Hill region shrinks to a point, while at $E = 4.5g$, it is a twice-punctured torus. Figure 2(b) illustrates the Hill region at $E = 4g$.

Low and high energy limits: In the CM frame, the 3 rotor problem (11) has a 4-dimensional phase space but possesses only one known conserved quantity (12). However, an extra conserved quantity emerges as $E \rightarrow 0$ or $E \rightarrow \infty$.

(a) For $E \gg g$, the kinetic energy dominates and $H \approx (p_1^2 - p_1 p_2 + p_2^2)/mr^2$. Here, $\varphi_{1,2}$ becomes cyclic coordinates and $p_{1,2}$ are both approximately conserved.

(b) For $E \ll g$, the system executes small oscillations around the ground state G ($\varphi_{1,2} \equiv 0$). The quadratic approximation to the Lagrangian (6) for relative motion is

$$L_{low} = (mr^2/3) [\dot{\varphi}_1^2 + \dot{\varphi}_2^2 + \dot{\varphi}_1 \dot{\varphi}_2] - g(\varphi_1^2 + \varphi_2^2 + \varphi_1 \varphi_2). \quad (17)$$

The linear equations of motion for φ_1 and φ_2 decouple,

$$mr^2 \ddot{\varphi}_1 = -3g\varphi_1 \quad \text{and} \quad mr^2 \ddot{\varphi}_2 = -3g\varphi_2, \quad (18)$$

leading to the separately conserved normal mode energies $E_{1,2} = (mr^2 \dot{\varphi}_{1,2}^2 + 3g\varphi_{1,2}^2)/2$. The equality of frequencies implies that any pair of independent linear combinations of φ_1 and φ_2 is also normal modes. Of particular significance are the coordinates $\varphi_{\pm} = (\varphi_1 \pm \varphi_2)/2$ that diagonalize the kinetic and potential energy quadratic forms,

$$L_{low} = mr^2 \dot{\varphi}_+^2 - 3g\varphi_+^2 + mr^2 \dot{\varphi}_-^2/3 - g\varphi_-^2. \quad (19)$$

Though (18) are simply the EOM for a pair of decoupled oscillators, the Lagrangian and Poisson brackets $\{\cdot, \cdot\}$ inherited from the nonlinear theory are different from the standard ones. With conjugate

momenta $p_{1,2} = (mr^2/3)(2\dot{\varphi}_{1,2} + \dot{\varphi}_{2,1})$, the Hamiltonian corresponding to (17) is

$$H_{low} = \frac{p_1^2 - p_1 p_2 + p_2^2}{mr^2} + g(\varphi_1^2 + \varphi_2^2 + \varphi_1 \varphi_2). \quad (20)$$

Here, $p_{1,2}$ differs from the standard momenta $p_{1,2}^s = mr^2 \dot{\varphi}_{1,2}$, whose PBs are now noncanonical, $\{\varphi_i, p_j^s\} = -1 + 3\delta_{ij}$. H_{low} , $L_z = mr^2(\varphi_1 \dot{\varphi}_2 - \varphi_2 \dot{\varphi}_1)$ and the normal mode energies,

$$H_{1,2} = (2p_{1,2} - p_{2,1})^2 / 2mr^2 + 3g\varphi_{1,2}^2/2, \quad (21)$$

are the obvious low energy constants of motion. Only three are independent due to the relation

$$H_{low} = \frac{2}{3} \left[H_1 + H_2 + \sqrt{H_1 H_2 - (3g/4mr^2)L_z^2} \right]. \quad (22)$$

IV. REDUCTION TO ONE DEGREE OF FREEDOM

Through a reduction to one degree of freedom, we find two families of periodic orbits, the pendula and isosceles breathers (see Fig. 3). They exist at all energies, go from librational to rotational motion as E increases and turn out to have remarkable stability properties.

A. Periodic pendulum solutions

We seek solutions where one pair of rotors forms a “bound state” with constant angular separation. Consistency requires this separation to vanish so that the two behave like a single rotor and the equations reduce to that of a two-rotor problem. There are three such families of “pendulum” solutions depending on which pair is bound [see Fig. 3(a)]. For definiteness, we suppose that the first two particles have a fixed separation ζ ($\theta_1 = \theta_2 + \zeta$ or $\varphi_1 = \zeta$). Substituting this in (7), we get a consistency condition and an evolution equation for φ_2 ,

$$2 \sin \zeta - \sin \varphi_2 + \sin(\zeta + \varphi_2) = 0 \quad \text{and} \quad mr^2 \ddot{\varphi}_2 = -g [2 \sin \varphi_2 - \sin \zeta + \sin(\zeta + \varphi_2)]. \quad (23)$$

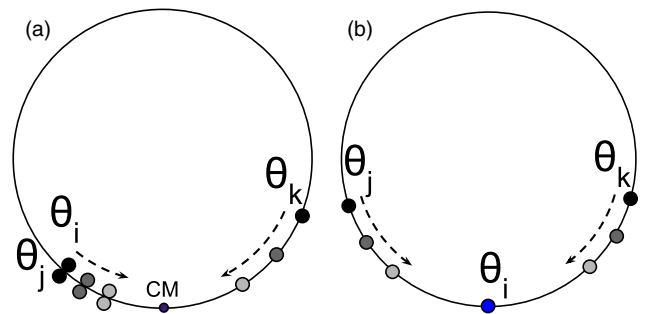


FIG. 3. (a) θ_i and θ_j form a molecule that along with θ_k oscillates about their common CM. (b) θ_i is at rest at the CM with θ_j and θ_k oscillating symmetrically about the CM. Here, i, j , and k denote any permutation of the numerals 1, 2, and 3. (a) Pendula, (b) Isosceles “breathers.”

The consistency condition is satisfied only when the separation $\zeta = 0$, i.e., rotors 1 and 2 must coincide so that $\varphi_1 = 0$ and $\dot{\varphi}_1 = 0$ (or $p_2 = 2p_1$) at all times (the other two families are defined by $\varphi_2 = \dot{\varphi}_2 = 0$ and $\varphi_1 + \varphi_2 = \dot{\varphi}_1 + \dot{\varphi}_2 = 0$). The evolution equation for φ_2 reduces to that for a pendulum,

$$mr^2\ddot{\varphi}_2 = -3g \sin \varphi_2 \quad \text{with} \quad E = \frac{mr^2\dot{\varphi}_2^2}{3} + 2g(1 - \cos \varphi_2) \quad (24)$$

being the conserved energy. The periodic solutions are either librational (for $0 \leq E < 4g$) or rotational (for $E > 4g$) and may be expressed in terms of the Jacobi elliptic function sn,

$$\bar{\varphi}_2(t) = \begin{cases} 2 \arcsin(k \operatorname{sn}(\omega_0 t, k)) & \text{for } 0 \leq E \leq 4g, \\ 2 \arcsin(\operatorname{sn}(\omega_0 t/\kappa, \kappa)) & \text{for } E \geq 4g. \end{cases} \quad (25)$$

Here, $\omega_0 = \sqrt{3g/mr^2}$ and the elliptic modulus $k = \sqrt{E/4g}$ with $\kappa = 1/k$. Thus $0 \leq k < 1$ for libration and $0 \leq \kappa < 1$ for rotation. The corresponding periods are $\tau_{\text{lib}} = 4K(k)/\omega_0$ and $\tau_{\text{rot}} = 2\kappa K(\kappa)/\omega_0$, where K is the complete elliptic integral of the first kind. As $E \rightarrow 4g^\pm$, the period diverges and we have the separatrix $\bar{\varphi}_2(t) = 2 \arcsin(\tanh(\omega_0 t))$. The conditions $\varphi_1 = 0$ and $p_2 = 2p_1$ define a 2d “pendulum submanifold” of the 4d phase space foliated by the above pendulum orbits. Upon including the CM motion of φ_0 , each of these periodic solutions may be promoted to a quasiperiodic orbit of the three-rotor problem. There is a two-parameter family of such periodic orbits, labeled for instance, by the relative energy E and the CM angular momentum p_0 .

1. Stability of pendulum solutions via monodromy matrix

Introducing the dimensionless variables

$$\tilde{p}_{1,2} = p_{1,2}/\sqrt{mr^2g} \quad \text{and} \quad \tilde{t} = t\sqrt{g/mr^2}, \quad (26)$$

the equations for small perturbations

$$\varphi_1 = \delta\varphi_1, \quad \varphi_2 = \bar{\varphi}_2 + \delta\varphi_2, \quad \text{and} \quad p_{1,2} = \bar{p}_{1,2} + \delta p_{1,2} \quad (27)$$

to the above pendulum solutions (25) to (11) are

$$\frac{d^2}{d\tilde{t}^2} \begin{pmatrix} \delta\varphi_1 \\ \delta\varphi_2 \end{pmatrix} = - \begin{pmatrix} 2 + \cos \bar{\varphi}_2 & 0 \\ \cos \bar{\varphi}_2 - 1 & 3 \cos \bar{\varphi}_2 \end{pmatrix} \begin{pmatrix} \delta\varphi_1 \\ \delta\varphi_2 \end{pmatrix}. \quad (28)$$

This is a pair of coupled Lamé-type equations since $\bar{\varphi}_2$ is an elliptic function. The analogous equation in the 2d anharmonic oscillator

reduces to a single Lamé equation.^{5,6} Our case is a bit more involved and we resort to a numerical approach here. It is convenient to consider the first order formulation

$$\frac{d}{d\tilde{t}} \begin{pmatrix} \delta\varphi_1 \\ \delta\varphi_2 \\ \delta\tilde{p}_1 \\ \delta\tilde{p}_2 \end{pmatrix} = - \begin{pmatrix} 0 & 0 & -2 & 1 \\ 0 & 0 & 1 & -2 \\ 1 + \cos \bar{\varphi}_2 & \cos \bar{\varphi}_2 & 0 & 0 \\ \cos \bar{\varphi}_2 & 2 \cos \bar{\varphi}_2 & 0 & 0 \end{pmatrix} \begin{pmatrix} \delta\varphi_1 \\ \delta\varphi_2 \\ \delta\tilde{p}_1 \\ \delta\tilde{p}_2 \end{pmatrix}. \quad (29)$$

Since $m, g,$ and r have been scaled out, there is no loss of generality in working in units where $m = g = r = 1$, as we do in the rest of this section. Though the coefficient matrix $A(t)$ is τ -periodic, the solutions satisfy $\psi(t + \tau) = M(\tau)\psi(t)$, where the eigenvalues λ of the monodromy matrix $M(\tau)$ are related to the Lyapunov exponents of pendula,

$$\mu = \lim_{t \rightarrow \infty} \frac{1}{t} \ln \frac{|\psi(t)|}{|\psi(0)|} \quad \text{via} \quad \mu = \frac{\log |\lambda|}{\tau}. \quad (30)$$

Since ours is a Hamiltonian system with two degrees of freedom, pendula are stable if the stability index $\sigma = \operatorname{tr} M - 2$ has magnitude ≤ 2 and are unstable otherwise.⁷

We now discuss the energy dependence of the stability index for pendula. In the limit of zero energy, (25) reduces to the ground state G and $A(t)$ becomes time-independent and similar to $2\pi i \times \operatorname{diag}(1, 1, -1, -1)$. Consequently, $M = \exp(A\tau)$ is the 4×4 identity I . Thus, G is stable and small perturbations around it are periodic with period $\tau = 2\pi/\omega_0$, as found in Eq. (16). For $E > 0$, we evaluate M numerically. We find it more efficient to regard M as the fundamental matrix solution to $\dot{\psi} = A(t)\psi$ rather than as a path ordered exponential or as a product of infinitesimal time-evolution matrices. Remarkably, as discussed below, we find that while the system is stable for low energies $0 \leq E \leq E_1^l \approx 3.99$ and high energies $E \geq E_1^r \approx 5.60$, the neighborhood of $E = 4$ consists of a doubly infinite sequence of intervals where the behavior alternates between stable and unstable (see Fig. 4). This is similar to the infinite sequence of transition energies for certain periodic orbits of a class of Hamiltonians studied in Ref. 8 and to the singly infinite sequence of transitions in the 2d anharmonic oscillator as the coupling α goes from zero to infinity,⁵

$$H_{\text{anharmon}} = \frac{1}{2}(p_1^2 + p_2^2) + \frac{1}{4}(q_1^4 + q_2^4) + \alpha q_1^2 q_2^2. \quad (31)$$

Stability of librational pendula ($E < 4$): In the first stable phase $0 \leq E \leq E_1^l$, $\phi = \arg \lambda_3$ monotonically increases from 0 to 2π

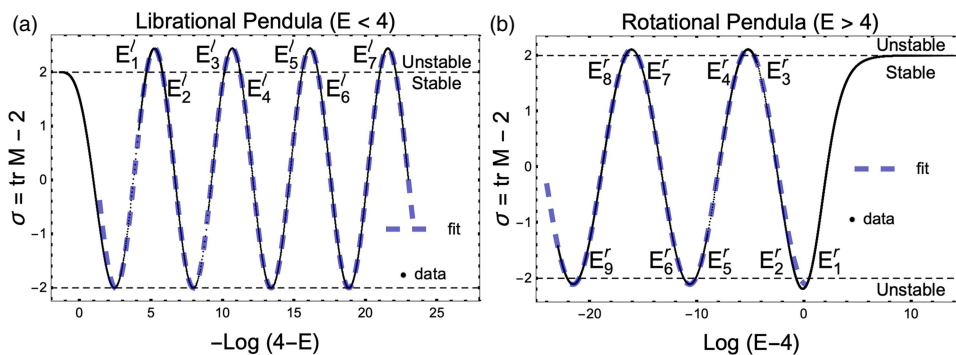


FIG. 4. Numerically obtained stability index of pendulum solutions showing approach to periodic oscillations between stable and unstable phases as $E \rightarrow 4^\pm$. Equations (33) and (36) are seen to fit the data as $E \rightarrow 4^\pm$.

with growing energy and $\lambda_4 = e^{-i\phi}$ goes round the unit circle once clockwise. There is a stable to unstable phase transition at E_1^ℓ . In the unstable phase $E_1^\ell < E < E_2^\ell$, $\sigma > 2$ corresponding to real positive λ_4 increasing from 1 to 1.9 and then dropping to 1 (see Fig. 4). There is then an unstable to stable transition at E_2^ℓ . This pattern repeats so that the librational regime $0 < E < 4$ is divided into an infinite succession of progressively narrower stable and unstable phases. Remarkably, we find that the stable phases asymptotically have equal widths on a log-arithmetic energy scale just as the unstable ones do. Indeed, if we let E_{2n+1}^ℓ and E_{2n}^ℓ denote the energies of the stable to unstable and unstable to stable transitions for $n = 1, 2, 3, \dots$, then the widths w_n^{lu} and w_{n+1}^{ls} of the n th unstable and $n + 1$ st stable phases are

$$\begin{aligned} w_n^{lu} &= E_{2n}^\ell - E_{2n-1}^\ell \approx (E_2^\ell - E_1^\ell) \times e^{-\Lambda(n-1)} \quad \text{and} \\ w_{n+1}^{ls} &= E_{2n+1}^\ell - E_{2n}^\ell \approx (E_3^\ell - E_2^\ell) \times e^{-\Lambda(n-1)}. \end{aligned} \tag{32}$$

Here, $E_2^\ell - E_1^\ell \approx e^{-4.67}(1 - e^{-1.11})$ and $E_3^\ell - E_2^\ell \approx e^{-5.78}(1 - e^{-4.34})$ are the lengths of the first unstable and second stable intervals, while $\Lambda \approx 1.11 + 4.34 = 5.45$ is the combined period on a log scale. The first stable phase has a width $E_1^\ell - 0 \approx 4 - e^{-4.67}$ that does not scale like the rest. Our numerically obtained stability index (see Fig. 4) is well approximated by

$$\sigma \approx 2.22 \cos \left[\frac{2}{\sqrt{3}} \log(4 - E) + 0.24 \right] + 0.22 \quad \text{as } E \rightarrow 4^- \tag{33}$$

On the other hand, $\sigma(E) \sim 2 - \mathcal{O}(E^3)$ when $E \rightarrow 0$.

Stability of rotational pendula ($E > 4$): For sufficiently high energies $E \geq E_1^r$, the rotational pendulum solutions are stable. In fact, as E decreases from ∞ to E_1^r , $\lambda_4 = e^{-i\phi}$ goes counterclockwise around the unit circle from 1 to -1 . There is a stable to unstable transition at E_1^r . As E decreases from E_1^r to E_2^r , λ_4 is real and negative, decreasing from -1 to -1.5 and then returning to -1 (see Fig. 4). This is followed by a stable phase for $E_2^r \geq E \geq E_3^r$, where λ_4 completes its passage counterclockwise around the unit circle reaching 1 at E_3^r . The last phase of this first cycle consists of an unstable phase between E_3^r and E_4^r where λ_4 is real and positive, increasing from 1 to 1.4 and then going down to 1. The structure of this cycle is to be contrasted with those in the librational regime where λ_4 made complete revolutions around the unit circle in each stable phase and was always positive in unstable phases. This is reflected in the stability index overshooting both 2 and -2 for rotational solutions but only exceeding 2 in the librational case. Furthermore, as in the librational case, there is an infinite sequence of alternating stable and unstable phases accumulating from above at $E = 4$, given by

$$\begin{aligned} \text{stable energies} &= [E_1^r, \infty) \bigcup_{n=1}^{\infty} [E_{2n+1}^r, E_{2n}^r] \quad \text{and} \\ \text{unstable energies} &= \bigcup_{n=1}^{\infty} (E_{2n}^r, E_{2n-1}^r). \end{aligned} \tag{34}$$

As before, with the exception of the two stable and one unstable intervals of highest energy, the widths of the stable and unstable intervals

are approximately constant on a log scale,

$$\begin{aligned} w_n^{ru} &= E_{2n-1}^r - E_{2n}^r \approx (E_3^r - E_4^r) \times e^{-\Lambda(n-2)} \quad \text{and} \\ w_{n+1}^{rs} &= E_{2n}^r - E_{2n+1}^r \approx (E_4^r - E_5^r) \times e^{-\Lambda(n-2)} \end{aligned} \tag{35}$$

for $n = 2, 3, 4, \dots$. Here, $E_3^r - E_4^r \approx e^{-4.7}(1 - e^{-1.1})$ and $E_4^r - E_5^r \approx e^{-5.8}(1 - e^{-4.3})$ are the lengths of the second unstable and third stable intervals, while $\Lambda \approx 1.1 + 4.3 = 5.4$ is the combined period. The three highest energy phases are anomalous: (a) $E \geq E_1^r \approx 5.60$ is a stable phase of infinite width, (b) the unstable phase $E_1^r > E > E_2^r \approx 4.48$ has width $1.2 > 1.1$ on a log scale and manifests more acute instability and (c) the stable phase $E_2^r \geq E \geq E_3^r \approx 4.01$ has a less than typical width $3.9 < 4.3$ (see Fig. 4). As before, we obtain the fit

$$\sigma \approx -2.11 \cos \left[\frac{1}{\sqrt{3}} \log(E - 4) - 0.12 \right] \quad \text{as } E \rightarrow 4^+, \tag{36}$$

while $\sigma(E) \sim 2 - \mathcal{O}(1/E)$ when $E \rightarrow \infty$.

Energy dependence of eigenvectors: Since the pendulum solutions form a one-parameter family of periodic orbits $(0, \varphi_2, p_1, 2p_1)$ with continuously varying time periods, a perturbation tangent to this family takes a pendulum trajectory to a neighboring pendulum trajectory and is therefore neutrally stable. These perturbations span the 1-eigenspace span (v_1, v_2) of the monodromy matrix, where $v_1 = (0, 1, 0, 0) = \partial_{\varphi_2}$ and $v_2 = (0, 0, 1, 2) = \partial_{p_1} + 2\partial_{p_2}$. The other two eigenvectors of M have a simple dependence on energy and thus help in ordering the eigenvalues λ_3 and λ_4 away from transitions. In the “unstable” energy intervals,

$$(E_1^\ell, E_2^\ell) \cup (E_2^r, E_1^r) \cup (E_3^\ell, E_4^\ell) \cup (E_4^r, E_3^r) \cup \dots, \tag{37}$$

$M = \text{diag}(1, 1, \lambda_3, 1/\lambda_3)$ in the basis (v_1, v_2, v_+, v_-) where $v_\pm = (2a(E), -a(E), \pm b(E), 0)$. In the same basis, $M = \text{diag}(1, 1, R_\phi)$ in the complementary “stable” energy intervals $(0, E_1^\ell) \cup (E_1^r, \infty) \cup \dots$. Here, R_ϕ is the 2×2 rotation matrix $(\cos \phi, \sin \phi | -\sin \phi, \cos \phi)$. At the transition energies, either a or b vanishes so that v_+ and v_- become collinear and continuity of eigenvectors with E cannot be used to unambiguously order the corresponding eigenvalues across transitions. For instance, the eigenvalue that went counterclockwise around the unit circle for $E < E_1^\ell$ could be chosen to continue as the real eigenvalue of magnitude either greater or lesser than one when E exceeds E_1^ℓ .

Pitfall in trigonometric and quadratic approximation at low energies: Interestingly, if for low energies ($E \ll g$), we use the simple harmonic/trigonometric approximation to (25), $\varphi_2 \approx \sqrt{E/g} \sin \omega_0 t$ with $\omega_0 = \sqrt{3g/mr^2}$ and $E \approx (mr^2/3)\dot{\varphi}_2^2 + g\bar{\varphi}_2^2$ and approximate $\cos \bar{\varphi}_2$ by $1 - \bar{\varphi}_2^2/2$ in (29), we find that the eigenvalues of the monodromy matrix are of the form $e^{\pm i\theta}$ and $e^{\pm i\phi}$ where θ and ϕ monotonically increase from zero with energy upto moderate energies. By contrast, as we saw above, two of the eigenvalues $\lambda_{1,2}$ are always equal to one, a fact which is not captured by this approximation.

B. Periodic isosceles “breather” solutions

We seek solutions where two of the separations remain equal at all times: $\theta_i - \theta_j = \theta_j - \theta_k$ where (i, j, k) is any permutation of $(1, 2, 3)$. Loosely, these are “breathers” where one rotor is always at rest midway between the other two [see Fig. 3(b)]. For definiteness,

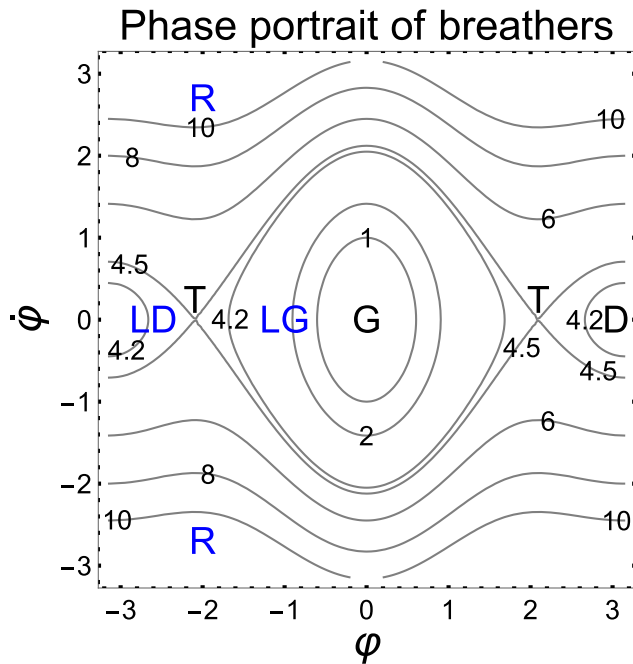


FIG. 5. Level contours of E on a phase portrait of the LG, LD, and R families of isosceles periodic solutions.

suppose $\theta_1 - \theta_2 = \theta_2 - \theta_3$ or equivalently $\varphi_1 = \varphi_2$. Substituting this in Eq. (7), we get a single evolution equation for $\varphi_1 = \varphi_2 = \varphi$,

$$mr^2\dot{\varphi} = -g(\sin \varphi + \sin 2\varphi), \tag{38}$$

which may be interpreted as a simple pendulum with an additional periodic force. As before, each periodic solution of this equation may, upon the inclusion of CM motion, be used to obtain quasiperiodic solutions of the three-rotor problem.

At $E = 0$, the isosceles solutions reduce to the ground state G. More generally, there are two families of librational breathers. With E denoting energy in units of g , they are LG [oscillations around G ($\varphi = 0$) for $0 \leq E \leq 9/2$] and LD [oscillations around D ($\varphi = \pi$) for $4 \leq E \leq 9/2$] with monotonically growing time period which diverges at the separatrix at $E = 9/2$ (see Fig. 5). For $E > 9/2$, we have rotational modes R with time period diminishing with energy [$\tau^{\text{rot}}(E) \sim 2\pi/\sqrt{E}$ as $E \rightarrow \infty$]. At very high energies, one rotor is at rest while the other two rotate rapidly in opposite directions. Equation (38) may be reduced to quadrature by the use of the conserved relative energy (9),

$$E = mr^2\dot{\varphi}^2 + g(3 - 2\cos \varphi - \cos 2\varphi). \tag{39}$$

For instance, in the case of the LG family,

$$\frac{\omega_0 t}{\sqrt{3}} = \frac{1}{\sqrt{2}} \int_0^u \frac{du}{\sqrt{u(2-u)(u^2 - 3u + E/2)}}, \tag{40}$$

where $u = 1 - \cos \varphi$. The relative angle φ may be expressed in terms of Jacobi elliptic functions. Substituting $\varepsilon = \sqrt{9 - 2E}$,

$$\begin{aligned} \varphi(t) &= \arccos \left(1 - \frac{E\eta^2}{2\varepsilon + (3 - \varepsilon)\eta^2} \right) \quad \text{where} \\ \eta(t) &= \text{sn} \left(\frac{\sqrt{\varepsilon}\omega_0 t}{\sqrt{3}}, \sqrt{\frac{(\varepsilon - 1)(3 - \varepsilon)}{8\varepsilon}} \right). \end{aligned} \tag{41}$$

It turns out that the periods of both LG and LD families are given by a common expression,

$$\tau^{\text{lib}}(E) = \frac{4\sqrt{3}}{\omega_0\sqrt{\varepsilon}} K \left(\sqrt{\frac{1}{2} - \frac{6-E}{4\varepsilon}} \right) \quad \text{for } 0 \leq E \leq 4.5. \tag{42}$$

As $E \rightarrow 4.5$, τ^{lib} diverges as $2\sqrt{2/3} \log(4.5 - E)$. The time period of rotational solutions (for $E \geq 4.5$) is

$$\tau^{\text{rot}}(E) = \frac{4\sqrt{3}}{\omega_0} (E^2 - 4E)^{-1/4} K \left(\sqrt{\frac{1}{2} + \frac{6-E}{2\sqrt{E^2 - 4E}}} \right). \tag{43}$$

Linear stability of breathers: The stability of isosceles solutions as encoded in the stability index ($\sigma = \text{tr } M - 2$) is qualitatively different from that of the pendulum solutions. In particular, there is only one unstable to stable transition occurring at $E \approx 8.97$ (see Fig. 6). Indeed, by computing the monodromies, we find that both families LG and LD of librational solutions are unstable. The stability index σ_{LG} grows monotonically from 2 to ∞ as the energy increases from 0 to 4.5. In particular, even though arbitrarily low energy breathers are small oscillations around the stable ground state G, they are themselves unstable to small perturbations. By contrast, we recall that low energy pendulum solutions around G are stable. On the other hand, the LD family of breathers is much more unstable, indeed, we find that σ_{LD} increases from $\approx 5.3 \times 10^4$ to ∞ for $4 < E < 4.5$. This is perhaps not unexpected, given that they are oscillations around the unstable static solution D. The rotational breathers are unstable for $4.5 < E < 8.97$ with σ_{R} growing from $-\infty$ to -2 . These

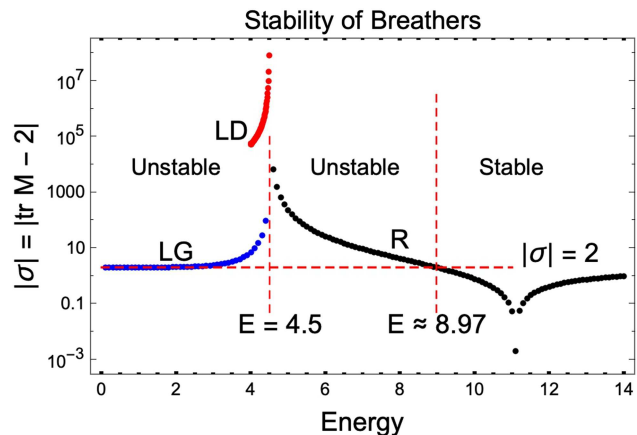


FIG. 6. Absolute value of the stability index of the isosceles breathers as a function of energy.

divergences of σ indicate that isosceles solutions around $E = 4.5$ suffer severe instabilities not seen in the pendulum solutions. Beyond $E = 8.97$, the rotational breathers are stable with σ_R growing from -2 to 2 as $E \rightarrow \infty$. This stability of the breathers is also evident from the Poincaré sections of Sec. VI. In fact, the isosceles solutions go from intersecting the Poincaré surface “ $\varphi_1 = 0$ ” at hyperbolic to elliptic fixed points as the energy is increased beyond $E \approx 8.97$ (see Figs. 9–11).

V. JACOBI-MAUPERTUIS METRIC AND CURVATURE

We now consider a geometric reformulation of the classical three-rotor problem that suggests the emergence of widespread instabilities for $E > 4$ from a largely stable phase at lower energies and a return to regularity as $E \rightarrow \infty$. This indicates the presence of an “order-chaos-order” transition which will be confirmed in Sec. VI.

It is well known that configuration space trajectories of the Lagrangian $L = (1/2)m_{ij}\dot{q}_i\dot{q}_j - V(q)$ may be regarded as reparametrized geodesics of the Jacobi-Maupertuis (JM) metric $g_{ij}^{JM} = (E - V)m_{ij}$ which is conformal to the mass/kinetic metric $m_{ij}(q)$.^{9,10} The sectional curvatures of this metric have information on the behavior of nearby trajectories with positive/negative curvature associated with (linear) stability/instability. For the three-rotor problem, the JM metric on the φ_1 - φ_2 configuration torus is given by

$$ds_{JM}^2 = \frac{2mr^2}{3}(E - V)(d\varphi_1^2 + d\varphi_1 d\varphi_2 + d\varphi_2^2), \quad (44)$$

where $V = g[3 - \cos \varphi_1 - \cos \varphi_2 - \cos(\varphi_1 + \varphi_2)]$. Letting f denote the conformal factor $E - V$ and using the gradient and Laplacian defined with respect to the flat kinetic metric, the corresponding scalar curvature ($2 \times$ the Gaussian curvature) is

$$R = \frac{|\nabla f|^2 - f \Delta f}{f^3} = \frac{g^2}{mr^2(E - V)^3} \left[6 + \left(\frac{2E}{g} - 3 \right) \left(3 - \frac{V}{g} \right) + \cos(\varphi_1 - \varphi_2) + \cos(2\varphi_1 + \varphi_2) + \cos(\varphi_1 + 2\varphi_2) \right]. \quad (45)$$

Behavior of JM curvature: For $0 \leq E \leq 4g$, R is strictly positive in the classically allowed Hill region ($V < E$) and diverges on the Hill boundary $V = E$ where the conformal factor vanishes (see Appendix A for a proof and the first two “bath-tub” plots of R in Fig. 7). Thus the geodesic flow should be stable for these energies. Remarkably, we also find a near absence of chaos in all Poincaré sections for $E \lesssim 3.8g$ (see Figs. 9 and 12). We will see that Poincaré

surfaces show significant chaotic regions for $E > 4g$. This is perhaps related to the instabilities associated with R acquiring both signs above this energy. Indeed, for $4g < E \leq 9g/2$, the above “bath-tub” develops sinks around the saddles $D(0, \pi)$, $D(\pi, 0)$, and $D(\pi, \pi)$, where R becomes negative, though it continues to diverge on the Hill boundary which is a union of two closed curves encircling the local maxima $T(\pm 2\pi/3, \pm 2\pi/3)$. For $E > 9g/2$, the Hill region expands to cover the whole torus. Here, though bounded, R takes either sign while ensuring that the total curvature $\int_{T^2} R \sqrt{\det g_{ij}} d\varphi_1 d\varphi_2$ vanishes. For asymptotically high energies, the JM metric tends to the flat metric $E m_{ij}$ and $R \sim 1/E^2 \rightarrow 0$ everywhere indicating a return to regularity.

JM stability of static solutions: The static solutions G, D, and T lie on the boundary of the Hill regions corresponding to the energies $E_{G,D,T} = 0, 4g$, and $4.5g$. We define the curvatures at G, D, and T by letting E approach the appropriate limiting values in the following formulas:

$$R_{(0,0)} = \frac{6g}{mr^2 E^2}, \quad R_{(0,\pi),(\pi,0),(\pi,\pi)} = \frac{-2g/mr^2}{(E - 4g)^2},$$

$$\text{and } R_{(\pm \frac{2\pi}{3}, \pm \frac{2\pi}{3})} = \frac{-12g/mr^2}{(2E - 9g)^2}. \quad (46)$$

Thus, $R_G = \infty$, while $R_D = R_T = -\infty$ indicating that G is stable, while D and T are unstable. These results on geodesic stability are similar to those obtained from (16). Note that we do not define the curvatures at G, D, and T by approaching these points from within the Hill regions as these limits are not defined for G and T and gives $+\infty$ for D. On the other hand, it is physically forbidden to approach the Hill boundary from the outside. Thus, we approach G, D, and T by varying the energy, while holding the location on the torus fixed.

VI. POINCARÉ SECTIONS: PERIODIC ORBITS & CHAOS

Here, we use Poincaré sections to study the transitions from regularity to chaos. By the Poincaré surface “ $\varphi_1 = 0$ ” at energy E (in units of g), we mean the 2d surface $\varphi_1 = 0$ contained in the corresponding 3d compact energy level set. It may be parametrized by φ_2 and p_2 with the two possible values of $p_1(\varphi_2, p_2; E)$ determined by energy. We record the points on the Poincaré surface where a trajectory that begins on it returns to it under the return map, thus obtaining a Poincaré section for the given initial condition (IC). A section is called regular if it consists of a finite set of points or is supported on a finite union of curves. Chaotic sections explore 2d

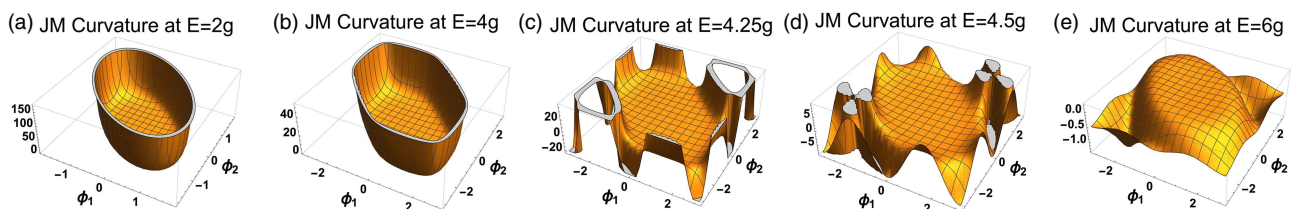


FIG. 7. Scalar curvature R of the JM metric on the Hill region of the φ_1 - φ_2 torus. In the regions shaded gray, $|R|$ is very large. We see that $R > 0$ for $E \leq 4g$ but has both signs for $E > 4g$ indicating instabilities.

regions. We define the chaotic region of a Poincaré surface at energy E to be the union of all chaotic sections at that energy.

A. Transition to chaos and global chaos

1. Numerical schemes and robustness of Poincaré sections

We implement the following numerical schemes: ODE45: explicit Runge-Kutta (RK) with difference order 5; RK4 and RK10: implicit RK with difference orders 4 and 10 and SPRK2: symplectic partitioned RK with difference order 2. Due to the accumulation of errors, different schemes (for the same ICs) sometimes produce trajectories that cease to agree after some time, thus reflecting the sensitivity to ICs. Despite this, we find that the corresponding Poincaré sections from all schemes are roughly the same when evolved for sufficiently long times (see Fig. 8). Moreover, we find a strong correlation between the degree to which different schemes produce the

same trajectory and the degree of chaos as manifested in Poincaré sections. As the agreement in trajectories between different schemes improves, the Poincaré sections go from chaotic to regular. Furthermore, for all ICs studied, the Poincaré sections on the surfaces $\varphi_1 = 0$, $\varphi_2 = 0$, $p_1 = 0$ and $p_2 = 0$ are qualitatively similar with regard to the degree of stochasticity. Thus, we restrict to the “ $\varphi_1 = 0$ ” Poincaré surface. The results presented below were obtained using the fastest of the schemes, namely, ODE45.

2. Symmetry breaking accompanying the onset of chaos

We find that for $E \lesssim 4$, all Poincaré sections (on the surface “ $\varphi_1 = 0$ ”) are nearly regular and display left-right ($\varphi_2 \rightarrow -\varphi_2$) and up-down ($p_2 \rightarrow -p_2$) symmetries (see Fig. 9). Though there are indications of chaos even at these energies along the periphery of the four stable lobes (e.g., near the unstable isosceles fixed points

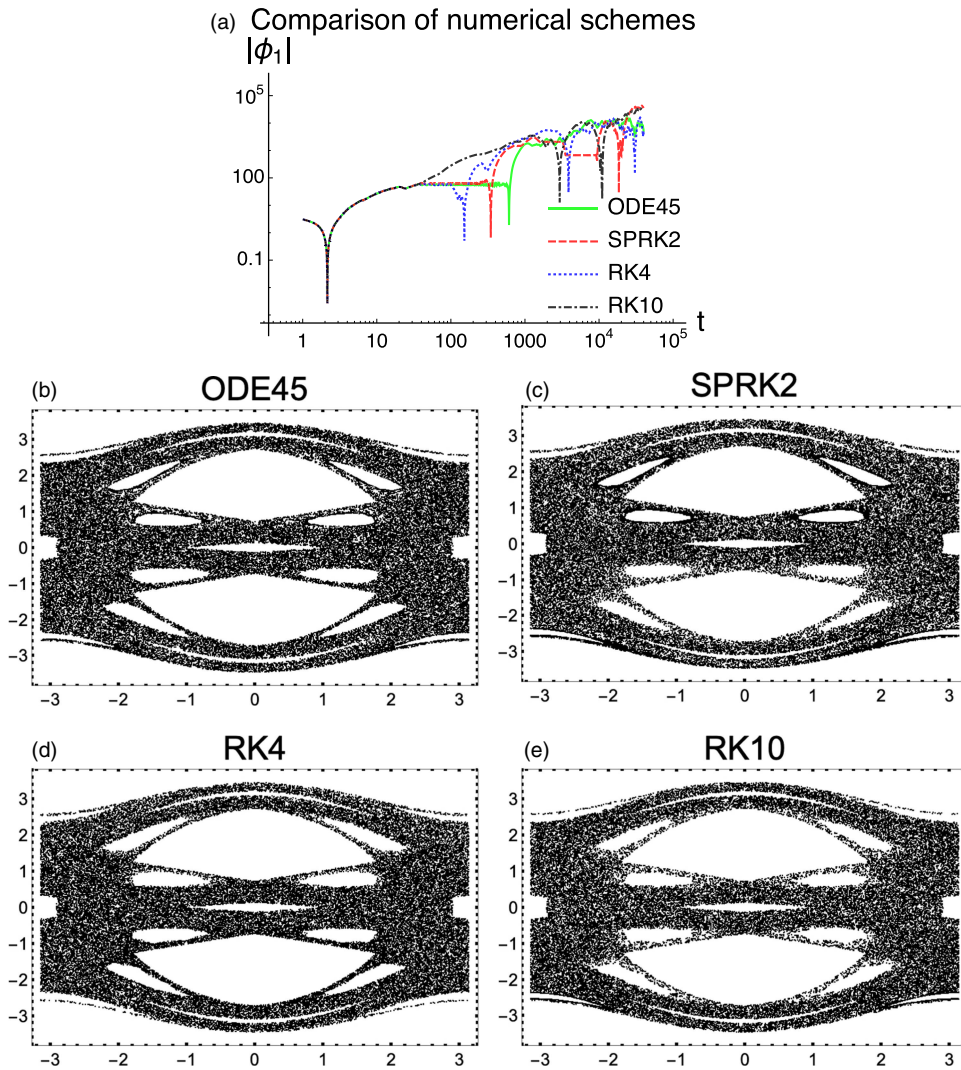


FIG. 8. (a) The trajectories (e.g., $|\varphi_1|$) obtained via different numerical schemes cease to agree after $t \sim 10^2$ for the IC $\varphi_1 = 6.23$, $\varphi_2 = 3.00$, $p_1 = -0.90$ and $p_2 = 1.87$ with $E = 9.98$. (b)–(e) However, Poincaré sections (with $\approx 5 \times 10^4$ points) obtained via different schemes are seen to explore qualitatively similar regions when evolved till $t = 10^5$ (though not for shorter times $\sim 10^3$).

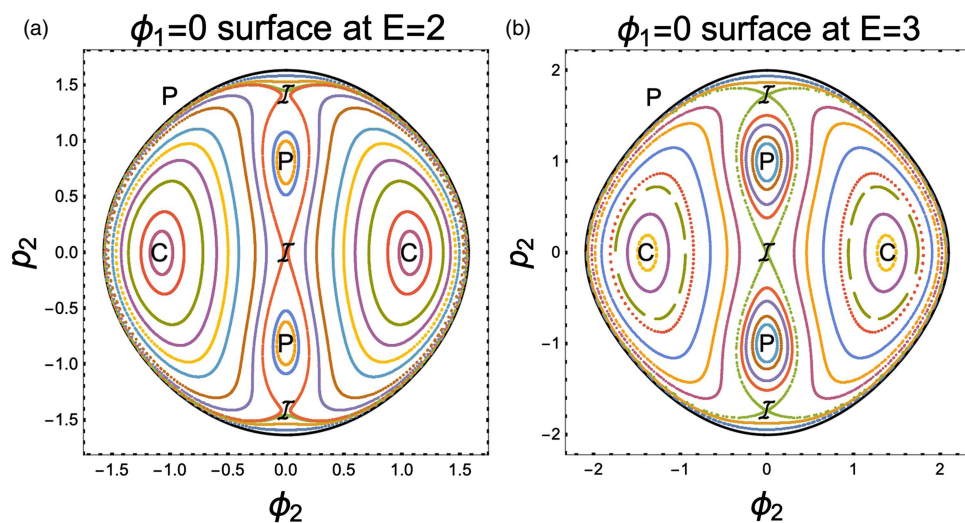


FIG. 9. Several Poincaré sections in the energetically allowed “Hill” region on the “ $\phi_1 = 0$ ” surface for $E = 2$ and 3. All sections (indicated by distinct colors online) are largely regular and possess up-down and left-right symmetries. The Hill boundary is the librational pendulum solution $\phi_1 = 0$. P, \mathcal{I} and C indicate pendulum, isosceles, and choreography periodic solutions. More careful examination of the vicinity of the \mathcal{I} s shows small chaotic sections.

\mathcal{I}), chaotic sections occupy a negligible portion of the Hill region. Chaotic sections make their first significant appearance at $E \approx 4$ along the figure-8 shaped separatrix and along the outer periphery of the regular “lobes” that flank it (see Fig. 10). This transition to chaos is accompanied by a spontaneous breaking of both the above symmetries. Interestingly, the $\phi_2 \rightarrow -\phi_2$ symmetry (though not $p_2 \rightarrow -p_2$) seems to be restored when $E \gtrsim 4.4$. The lack of $p_2 \rightarrow -p_2$ symmetry at high energies is not unexpected: rotors at high energies either rotate clockwise or counterclockwise.

At moderate energies $E \gtrsim 4$, we observe that all chaotic sections (irrespective of the ICs) occupy essentially the same region, as typified by the examples in Fig. 11. At somewhat higher energies (e.g., $E = 14$), we find chaotic sections that fill up both the entire

chaotic region and portions thereof when trajectories are evolved up to $t = 10^5$. At yet higher energies [e.g., $E = 18$, Fig. 11(e)], there is no single chaotic section that occupies the entire chaotic region as the $p_2 \rightarrow -p_2$ symmetry is broken.

3. Fraction of chaos and global chaos

For a range of energies beyond 4, we find that the area of the chaotic region increases with E (see Figs. 10 and 11). At $E \approx 5.5$, the chaotic region coincides with the energetically allowed portion of the Poincaré surface [see Fig. 11(c)]. Beyond this energy, chaotic sections are supported on increasingly narrow bands [see Fig. 11(e)]. This progression toward regularity is expected since the

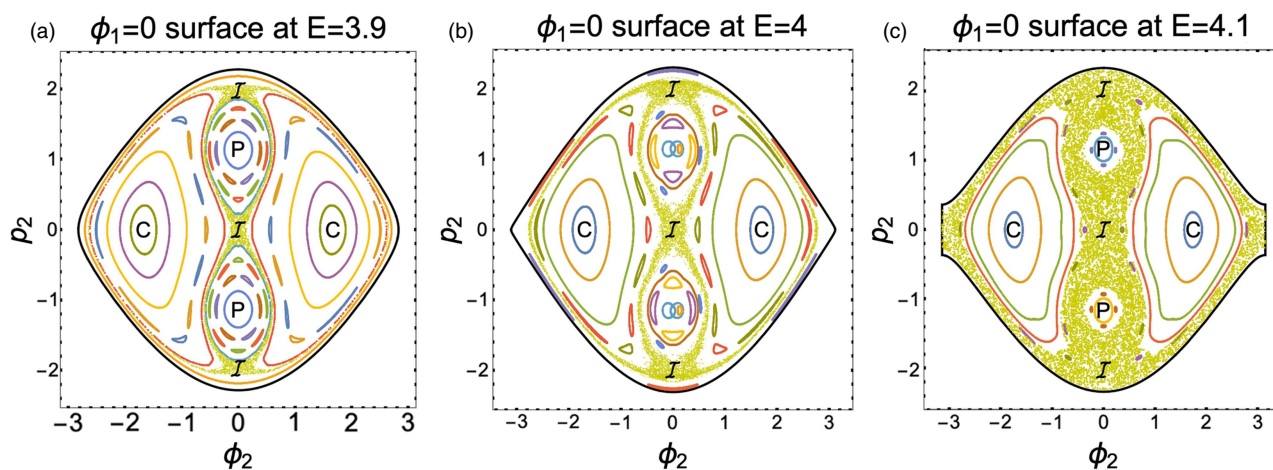


FIG. 10. Several Poincaré sections on the “ $\phi_1 = 0$ ” surface in the vicinity of $E = 4$ where the chaotic region (shaded, yellow online) makes its first significant appearance. Distinct sections have different colors online. On each surface, one sees breaking of both up-down and left-right symmetries. Apart from a couple of exceptions on the $E = 4$ surface, the set of ICs is left-right and up-down symmetric. The boundary of the Hill region on the “ $\phi_1 = 0$ ” Poincaré surface is the $\phi_1 = 0$ pendulum solution. It becomes disconnected for $E > 4$ owing to the bifurcation of the librational pendula into clockwise and counterclockwise rotational pendula.

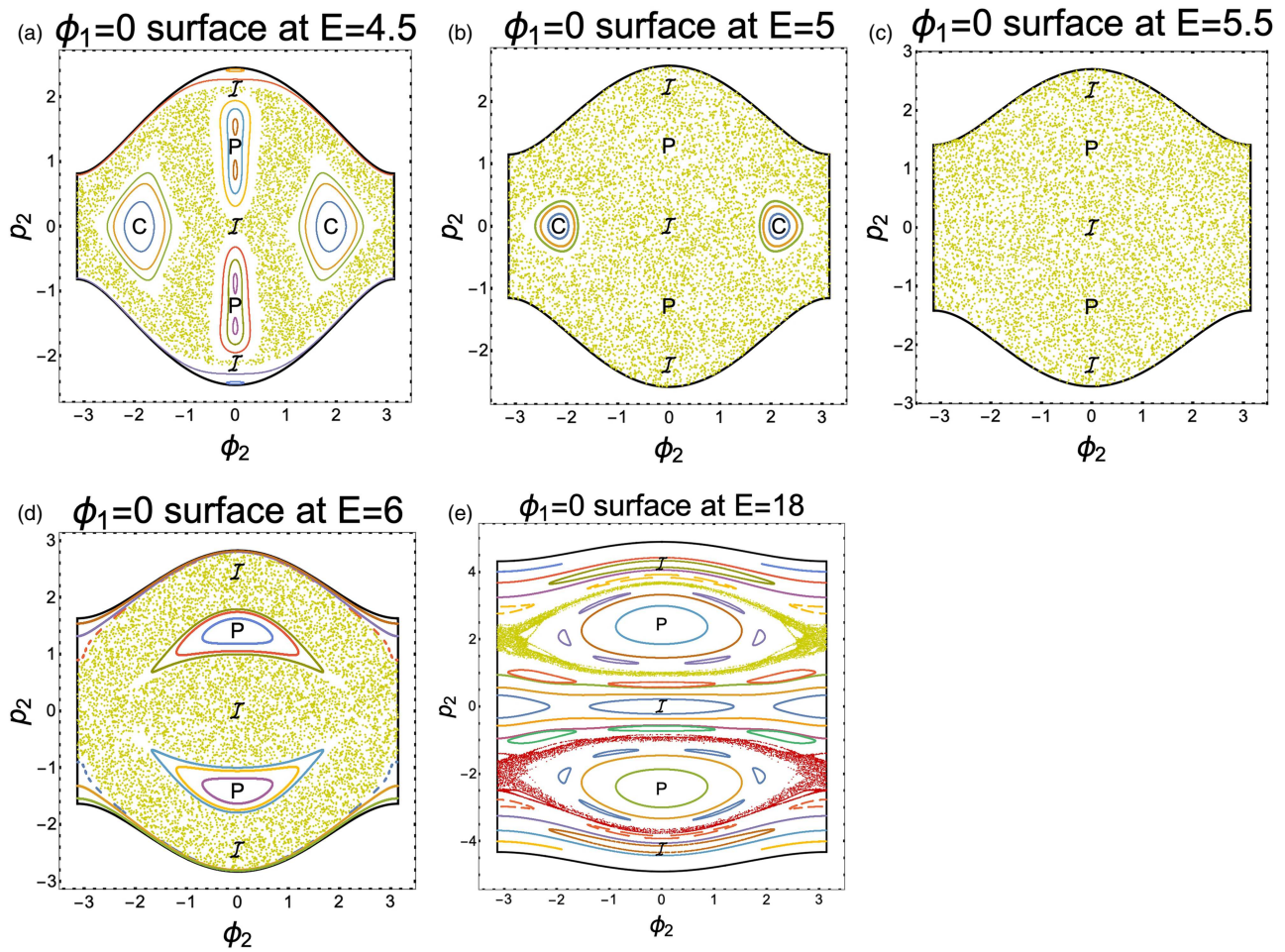


FIG. 11. The up-down symmetry remains broken, though the left-right symmetry is restored on Poincaré plots at higher energies. The periodic orbits corresponding to points marked C are choreographies for $E \lesssim 5.33$.

system acquires an additional conserved quantity in the limit $E \rightarrow \infty$. To quantify these observations, we find the “fraction of chaos” f by exploiting the feature that the density of points in chaotic sections is roughly uniform for all energies on the “ $\varphi_1 = 0$ ” surface (this is not true for most other Poincaré surfaces). Thus, f is estimated by calculating the fraction of the area of the Hill region covered by chaotic sections (see Appendix B and Fig. 12).

The near absence of chaos is reflected in f approximately vanishing for $E \lesssim 3.8$. There is a rather sharp transition to chaos around $E \approx 4$ ($f \approx 4\%$, 20% , and 40% at $E = 3.85$, 4 , and 4.1 ; see the lower inset of Fig. 12). This is a bit unexpected from the viewpoint of the KAM theory and might encode a novel mechanism by which KAM tori break down in this system. Thereafter, f rapidly rises and reaches the maximal value $f \approx 1$ at $E \approx 5.33$. As illustrated in the upper inset of Fig. 12, this “fully chaotic” phase persists up to $E \approx 5.6$. Interestingly, we find that for this range of energies, $f \approx 1$ on a variety of Poincaré surfaces examined (see Fig. 13), so that this may be regarded as a phase of “global chaos.” Furthermore, the density of points is

uniform on all Poincaré surfaces in this phase of global chaos indicating some sort of ergodicity. Additionally, the pendula and breathers are unstable in this phase (see Sec. IV) and it would be interesting to know whether this is the case with all periodic solutions. Remarkably, the cessation of the band of global chaos happens to coincide with the energy $E_1^r \approx 5.6$ above which pendulum solutions are always stable (see Fig. 4). Beyond $E \approx 5.6$, f decreases gradually to zero as $E \rightarrow \infty$. Interestingly, the sharp transition to chaos at $E \approx 4$ is also reflected in the JM curvature of Sec. V going from being positive for $E < 4$ to admitting both signs for $E > 4$. It is noteworthy that the stable to unstable transition energies in pendula also accumulate from both sides at $E = 4$ (see Fig. 4).

B. Periodic solutions on the Poincaré surface “ $\varphi_1 = 0$ ”

Here, we identify the points on the Poincaré surface corresponding to the periodic pendulum and isosceles solutions. Remarkably, careful examination of the Poincaré sections also leads us to a new

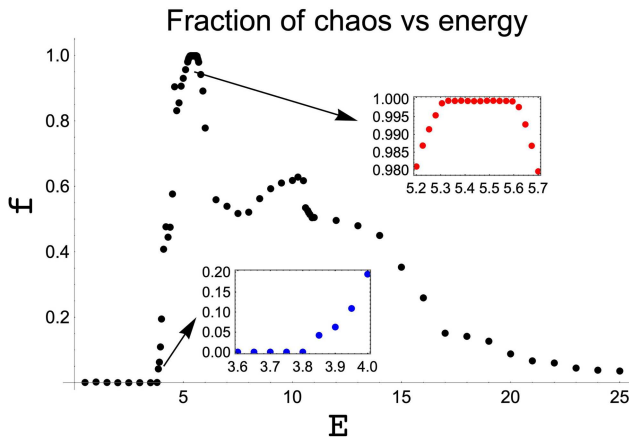


FIG. 12. Energy dependence of the area of the chaotic region on the “ $\varphi_1 = 0$ ” Poincaré surface as a fraction of the area of the Hill region.

family of periodic “choreography” solutions which are defined and discussed further in Sec. VII.

Pendula: The $\varphi_1 = 0$ pendulum solutions are everywhere tangent to the Poincaré surface “ $\varphi_1 = 0$ ” and interestingly constitute the “Hill” energy boundary (see Figs. 9–11). [Nb. This connection between pendulum solutions and the Hill boundary is special to the surfaces “ $\varphi_1 = 0$ ” and “ $\varphi_2 = 0$.”] By contrast, the other two classes of pendulum trajectories ($\varphi_2 = 0$ and $\varphi_1 + \varphi_2 = 0$) are transversal to this surface, meeting it at the pendulum points $P(0, \pm\sqrt{E/3})$ halfway to the boundary from the origin. These are period-2 and period-1 fixed points for librational and rotational solutions, respectively. Examination of the Poincaré sections indicates that pendulum solutions must be stable for $E \lesssim 3.9$ and $E \gtrsim 5.6$ leaving open the question of their stability at intermediate energies. As discussed in Sec. IV A, the pendula go from being stable to unstable infinitely often as $E \rightarrow 4^\pm$. Additionally, by considering initial conditions near the pendulum points, we find that the pendulum solutions lie within the large chaotic section only between $E \approx 4.6$ and the cessation of global chaos at $E \approx 5.6$.

Breathers: Unlike pendula, all isosceles breathers intersect the “ $\varphi_1 = 0$ ” surface transversally at points on the vertical axis. Indeed, the breathers defined by $\varphi_1 = \varphi_2$ and $\varphi_2 + 2\varphi_1 = 0$ intersect the surface at the isosceles points $\mathcal{I}(0, \pm\sqrt{E})$ which form a pair of period-2 fixed points for $E < 4.5$ and become period-1 in the rotational regime (see Figs. 9–11). The breathers defined by $\varphi_1 + 2\varphi_2 = 0$ intersect the surface at the period-1 fixed point at the origin. In agreement with the conclusions of Sec. IV B, the Poincaré sections show that all three isosceles points are unstable at low energies, lie in the large chaotic section for $3.9 \lesssim E \lesssim 8.97$ and are stable at higher energies.

A new family of periodic solutions: The period-2 fixed points C at the centers of the right and left lobes on the Poincaré surfaces of Figs. 9 and 10 correspond to a new family of periodic solutions. Evidently, they go from being stable to unstable as the energy crosses $E \approx 5.33$. We argue in Sec. VII that they are choreographies for $E \lesssim 5.33$.

VII. CHOREOGRAPHIES

Choreographies are an interesting class of periodic solutions of the n -body problem where all particles follow the same closed curve equally separated in time.¹¹ The Lagrange equilateral solution where three equal masses move on a common circle and the stable zero-angular momentum figure-8 solution discovered by Moore¹² (see also Ref. 13) are perhaps the simplest examples of choreographies in the equal mass gravitational 3 body problem. Here, we consider choreographies in the 3 rotor problem where the angles $\theta_i(t)$ of the three rotors may be expressed in terms of a single 3τ -periodic function, say $\theta_1(t)$,

$$\theta_2(t) = \theta_1(t + \tau) \text{ and } \theta_3(t) = \theta_1(t + 2\tau). \quad (47)$$

This implies that the CM and relative coordinates $\varphi_0, \varphi_1(t)$ and $\varphi_2(t) = \varphi_1(t + \tau)$ must be 3τ periodic [see Fig. 14(a)] and satisfy the delay algebraic equation

$$\begin{aligned} &\varphi_1(t) + \varphi_1(t + \tau) + \varphi_1(t + 2\tau) \\ &= \theta_1 - \theta_2 + \theta_2 - \theta_3 + \theta_3 - \theta_1 \equiv 0 \pmod{2\pi}. \end{aligned} \quad (48)$$

The EOM (7) become $3mr^2\ddot{\varphi}_0 = 0$ and the pair of delay differential equations

$$\begin{aligned} mr^2\ddot{\varphi}_1(t) = &-g[2 \sin \varphi_1(t) - \sin \varphi_1(t + \tau) \\ &+ \sin(\varphi_1(t) + \varphi_1(t + \tau))] \text{ and} \end{aligned} \quad (49)$$

$$\begin{aligned} mr^2\ddot{\varphi}_2(t) = &mr^2\ddot{\varphi}_1(t + \tau) = -g[2 \sin \varphi_1(t + \tau) \\ &- \sin \varphi_1(t) + \sin(\varphi_1(t) + \varphi_1(t + \tau))]. \end{aligned}$$

In fact, the second equation in (49) follows from the first by use of the delay algebraic equation (48). Moreover, using the definition of φ_0 , the constant angular velocity of the CM

$$\begin{aligned} \dot{\varphi}_0 &= \frac{1}{\tau} [\varphi_0(t + \tau) - \varphi_0(t)] \\ &= -\frac{1}{3\tau} [\varphi_1(t) + \varphi_1(t + \tau) + \varphi_1(t + 2\tau)]. \end{aligned} \quad (50)$$

It is verified that any 3τ periodic triple $\varphi_{0,1,2}$ satisfying (48), (49), and (50) leads to a choreography of the 3-rotor system. Thus, to discover a choreography, we only need to find a 3τ -periodic function φ_1 satisfying (48) and the first of the delay differential Eq. (49) with the period 3τ self-consistently determined. Now, it is easy to show that choreographies cannot exist at asymptotically high (relative) energies. In fact, at high energies, we may ignore the interaction terms ($\propto g$) in (49) to get $\varphi_1(t) \approx \omega t + \varphi_1(0)$ for $|\omega| \gg 1$. However, this is inconsistent with (48) which requires $3\omega t \equiv 0 \pmod{2\pi}$ at all times. On the other hand, as discussed below, we do find examples of choreographies at low and moderate relative energies.

A. Examples of choreographies

Uniformly rotating (at angular speed Ω) versions of the static solutions G and T (but not D) (see Fig. 1) provide the simplest examples of choreographies with $\theta_1(t) = \Omega t$ and $\tau = 2\pi/\Omega$ for G and $\tau = 2\pi/3\Omega$ for T where Ω is arbitrary. In the case of G, though all particles coincide, they may also be regarded as separated by τ . The

Global chaos at E = 5.516

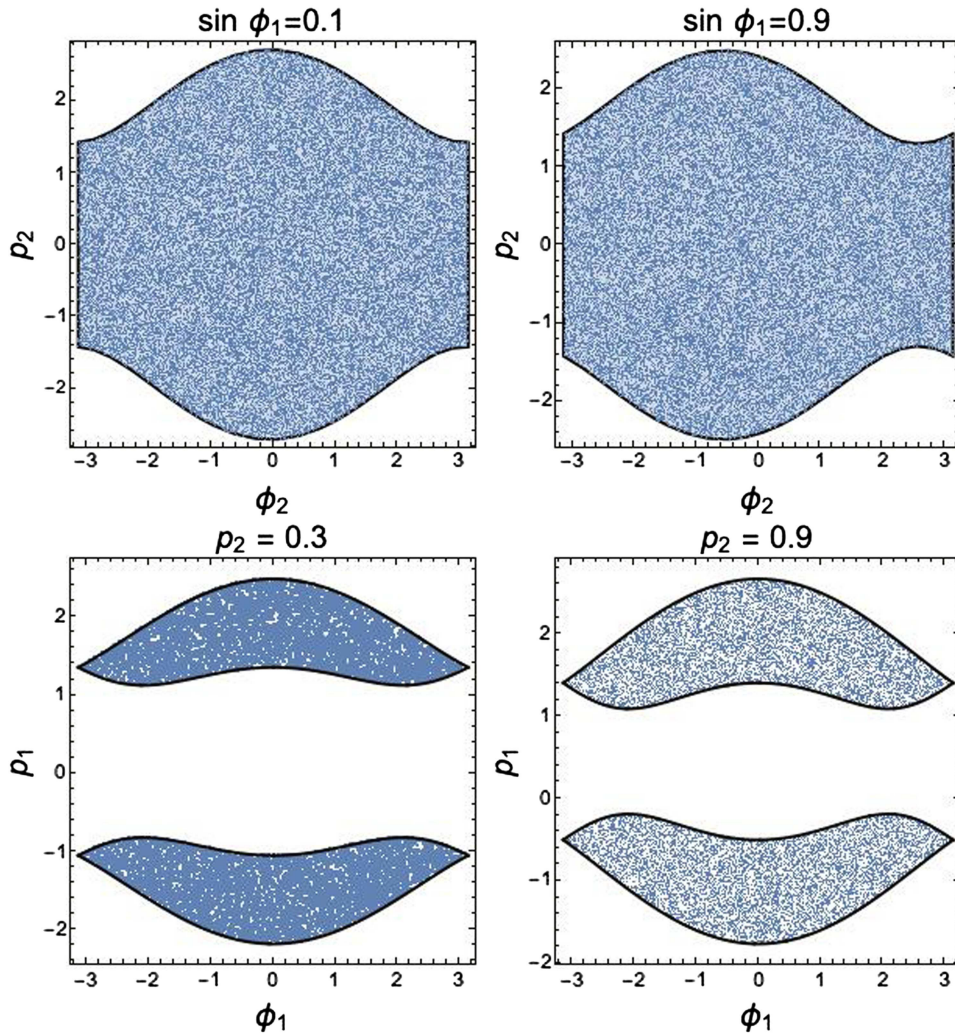


FIG. 13. Various Poincaré surfaces showing global chaos at E = 5.516.

energies (9) of these two families of choreographies come from the uniform CM motion and a constant relative energy:

$$E_{\text{tot}}^{(G)} = \frac{3}{2}mr^2\Omega^2 \quad \text{and} \quad E_{\text{tot}}^{(T)} = \frac{3}{2}mr^2\Omega^2 + \frac{9g}{2}. \quad (51)$$

These two families of choreographies have the scaling property: if $\theta(t)$ with period 3τ describes a choreography in the sense of (47), then $\theta(at)$ with period $|3\tau/a|$ also describes a choreography for any real a . It turns out that the above two are the only such “scaling” families of choreographies. To see this, we note that both $\theta(t)$ and $\theta(at)$ must satisfy the delay differential equation

$$\ddot{\theta}(t + \tau) - \ddot{\theta}(t) = \frac{-g}{mr^2} \left[2 \sin(\theta(t + \tau) - \theta(t)) - \sin(\theta(t) - \theta(t - \tau)) + \sin(\theta(t + \tau) - \theta(t - \tau)) \right], \quad (52)$$

implying that either $a^2 = 1$ or $\ddot{\theta}(t + \tau) = \ddot{\theta}(t)$. However, the latter implies that $\dot{\theta}(t + \tau) - \dot{\theta}(t) = -\dot{\varphi}_1(t)$ is a constant which must vanish for the delay algebraic equation (48) to be satisfied. Consequently, φ_2 must also vanish implying that the choreography is a uniformly rotating version of G or T.

B. Nonrotating choreographies

Remarkably, we have found another 1-parameter family of choreographies [e.g., Fig. 14(a)] that start out as small oscillations around G. At low energies, they have a period $3\tau = 2\pi/\omega_0$ and reduce to

$$\varphi_1(t) \approx \sqrt{\frac{2E}{3g}} \sin(\omega_0(t - t_0)) \quad \text{for} \quad E \ll g, \quad (53)$$

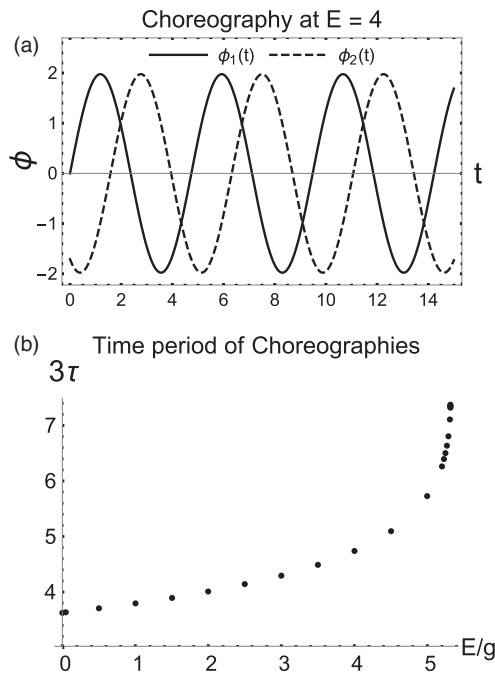


FIG. 14. (a) A nonrotating choreography at $E = 4g$ showing that the time lag between φ_1 and φ_2 is one-third the period. (b) The time period 3τ of nonrotating choreographies as a function of energy indicating divergence at $E \approx 5.33g$.

where $\omega_0 = \sqrt{3g/mr^2}$. It is easily verified that (48) is identically satisfied while (49) is satisfied for $E \ll g$. Moreover, using (50), we find that the angular speed $\dot{\varphi}_0$ of the CM must vanish for (53) so that the energy is purely from the relative motion. The phase trajectory corresponding to (53) intersects the $\varphi_1 = 0$ Poincaré surface at the pair of period-2 fixed points $C(\pm\sqrt{E/2g}, 0)$ which lie at the centers of the left and right stable “lobes” pictured in Fig. 9 at $E = 2g$ and $3g$.

More generally, we numerically find that when the ICs are chosen at the stable fixed points at the centers of these lobes, the trajectories are a one-parameter family of choreographies $\varphi_1(t; E)$ varying continuously with E up to $E \approx 5.33$. It can be argued that these choreographies are nonrotating (involve no CM motion). Indeed, from (50) and (48), we must have $3\tau\dot{\varphi}_0 \equiv 0 \pmod{2\pi}$, implying that $\dot{\varphi}_0$ cannot jump discontinuously. Since, $3\tau\dot{\varphi}_0 = 0$ as $E \rightarrow 0$ (53), it must remain zero when E is continuously increased from 0 to 5.33. Though we do not study their stability here by the monodromy approach, the Poincaré sections (see Figs. 9 and 10) indicate that they are stable. As shown in Fig. 14(b), the time period 3τ grows monotonically with E and appears to diverge at $E \approx 5.33$, which coincides with the beginning of the band of “global chaos” (see Sec. VI). For $E \gtrsim 5.33$, the period-2 choreography points C on the “ $\varphi_1 = 0$ ” Poincaré surface become unstable and lie in a chaotic region (see Fig. 11), preventing us from finding such a choreography, if it exists, using the above numerical technique. As argued before, choreographies are forbidden at very high energies. For instance, on the “ $\varphi_1 = 0$ ” Poincaré surface at $E = 18$ [see Fig. 11(e)], the analogs of the C points correspond

to unstable periodic orbits which are *not* choreographies. In fact, we conjecture that this family of periodic solutions ceases to be a choreography beyond $E \approx 5.33$.

VIII. DISCUSSION

In this paper, we have studied the classical three-rotor problem and found novel signatures of its transition to chaos as well as a phase of global chaos. We also discovered “pendulum” and “isosceles-breather” periodic solutions as well as choreographies and discussed their stability properties. Section I contains a concise summary of our results. Here, we discuss some open questions arising from our work.

Though Poincaré sections indicate that the center of mass dynamics of the three-rotor problem cannot possess any conserved quantity other than energy, it would be reassuring to demonstrate this. Analogously, the extension to our system, of Ziglin’s and Melnikov’s arguments for nonintegrability is also of interest.^{14,15}

While we found the trace of the monodromy for periodic “pendulum” solutions numerically, it would be interesting to prove the accumulation of stable to unstable phase transitions at $E = 4g$ as in Ref. 8 and establish its asymptotic periodicity on a log scale, for instance by finding an analytical expression for the stability index as Yoshida⁵ does in the 2d anharmonic oscillator of Eq. (31). It would also be interesting to explore a possible connection between this accumulation of transitions and the accumulation of homoclinic points at a hyperbolic fixed point in a chaotic system. The nature of bifurcations⁶ and local scaling properties¹⁶ at these transitions are also of interest. In another direction, one would like to understand if there is any connection between the accumulation of transition energies and the change in topology of the Hill region ($V \leq E$) of the configuration torus as E crosses the value $4g$ at the three critical points (saddles D) of the Morse function V (see Sec. III). One would also like to analyze the onset of widespread chaos in this system using methods such as those of Chirikov¹⁷ and Greene.¹⁸

We have argued that the 3 rotor system is integrable at $E = 0$ and ∞ ($g = \infty, 0$), where additional conserved quantities emerge. One wonders whether it is “integrable” at any other energy. In other words, is there any nontrivial energy hypersurface in phase space on which all trajectories are periodic or quasiperiodic so that the corresponding Poincaré sections are regular? Our estimate of the fraction of chaos on the “ $\varphi_1 = 0$ ” Poincaré surface strongly suggests that any integrable energy E_1 is either isolated or $E_1 \lesssim 3.8g$. However, even for low energies, we expect chaotic sections in the neighborhood of the isosceles points \mathcal{I} (see Fig. 9). In fact, we conjecture that the 3 rotor problem has no nontrivial integrable energies unlike the 2d anharmonic oscillator.⁵

As discussed in Sec. VI, Poincaré sections suggest a band of global chaos for $5.33g \lesssim E \lesssim 5.6g$. This is of course consistent with the instability of pendulum and breather solutions in this energy interval. Consequently, it would be interesting to investigate the possible ergodic behavior of three rotors for such energies.

Finally, a deeper understanding of the physical mechanisms underlying the onset of chaos in this system would be desirable, along with an examination of quantum manifestations of the classical chaos, given the connection to modeling chains of coupled Josephson junctions.

ACKNOWLEDGMENTS

We thank K. G. Arun, M. Berry, A. Chenciner, S. Dattagupta, S. R. Jain, A. Lakshminarayan, R. Nityananda, T. R. Ramadas, M. S. Santhanam, and anonymous reviewers for helpful comments and references. This work was supported in part by the Infosys Foundation, J N Tata trust under Grant Nos. MTR/2018/000734 and CRG/2018/002040 from the Science and Engineering Research Board, Government of India.

APPENDIX A: POSITIVITY OF JM CURVATURE FOR $0 \leq E \leq 4g$

Here, we prove that for $0 \leq E \leq 4g$, the JM curvature R of Sec. V is strictly positive in the Hill region ($E > V$) of the φ_1 - φ_2 configuration torus. It is negative outside and approaches $\pm\infty$ on the Hill boundary $E = V$. It is convenient to work in coordinates $\varphi_{\pm} = (\varphi_1 \pm \varphi_2)/2$ and define $P = \cos \varphi_+$ and $Q = \cos \varphi_-$. In these variables,

$$R = \frac{g^2 \mathcal{N}_E(P, Q)}{mr^2(E - V)^3} \quad \text{where} \quad \mathcal{N}_E = 5 + 2Q^2 - 6PQ + 8P^3Q + \left[\frac{2E}{g} - 3 \right] (2P^2 + 2PQ - 1). \tag{A1}$$

Since $E - V > 0$ in the Hill region, it suffices to show that $\mathcal{N}_E \geq 0$ on the whole torus and strictly positive in the Hill region. It turns out that (a) $\mathcal{N}_E \geq 0$ for $E = 0$ and $4g$ and (b) for $E = 0$, \mathcal{N}_E vanishes only at the ground state G while for $E = 4g$, it vanishes only at the saddles D, with both G and the Ds lying on the Hill boundary. Since G is distinct from the Ds, linearity of \mathcal{N}_E then implies that $\mathcal{N}_E > 0$ on the entire torus for $0 < E < 4g$. It only remains to prove (a) and (b).

To proceed, we regard \mathcal{N}_E as a function of the $[-1, 1] \times [-1, 1]$ PQ-square. (i) When $E = 0$, \mathcal{N}_0 has only one local extremum in the interior of the PQ-square at $(0, 0)$ where $\mathcal{N}_0(0, 0) = 8$. On the boundaries of the PQ-square,

$$\begin{aligned} \mathcal{N}_0(\pm 1, Q) &= 2(1 \mp Q)^2 \geq 0 \quad \text{and} \\ \mathcal{N}_0(P, \pm 1) &= 2(P \mp 1)^2(5 \pm 4P) \geq 0 \end{aligned} \tag{A2}$$

with \mathcal{N}_0 vanishing only at $(1, 1)$ and $(-1, -1)$ both of which correspond to G. Thus, $\mathcal{N}_0 \geq 0$ on the whole torus and vanishes only at G which lies on the Hill boundary. (ii) When $E = 4g$, the local extrema in the interior of the PQ-square are at $(0, 0)$ and $(\pm 1, \mp 5/3)/\sqrt{3}$, where \mathcal{N}_{4g} takes the values 0 and $40/27$. On the boundaries of the PQ-square,

$$\begin{aligned} \mathcal{N}_{4g}(\pm 1, Q) &= 2(1 \pm Q)(5 \pm Q) \geq 0 \quad \text{and} \\ \mathcal{N}_{4g}(P, \pm 1) &= 2(1 \pm P)(1 \pm P + 4P^2) \geq 0 \end{aligned} \tag{A3}$$

with \mathcal{N}_{4g} vanishing only at $(1, -1)$ and $(-1, 1)$. Hence, for $E = 4g$, $\mathcal{N}_{4g} \geq 0$ on the whole torus and vanishes only at the three saddle points (Ds) all of which lie on the Hill boundary.

APPENDIX B: MEASURING AREA OF CHAOTIC REGION ON “ $\varphi_1 = 0$ ” POINCARÉ SURFACE

To estimate the fraction of the area of the Hill region (at a given E) occupied by the chaotic sections on the “ $\varphi_1 = 0$ ” Poincaré surface, we need to assign an area to the corresponding scatterplot (e.g., see Fig. 11). We use the DelaunayMesh routine in Mathematica to triangulate the scatterplot so that every point in the chaotic region lies at the vertex of one or more triangles (see Fig. 15). For such a triangulation and a given $d > 0$, the d -area of the chaotic region is defined as the sum of the areas of those triangles with maximal edge length $\leq d$ (accepted triangles in Fig. 15). Figure 16 shows that the

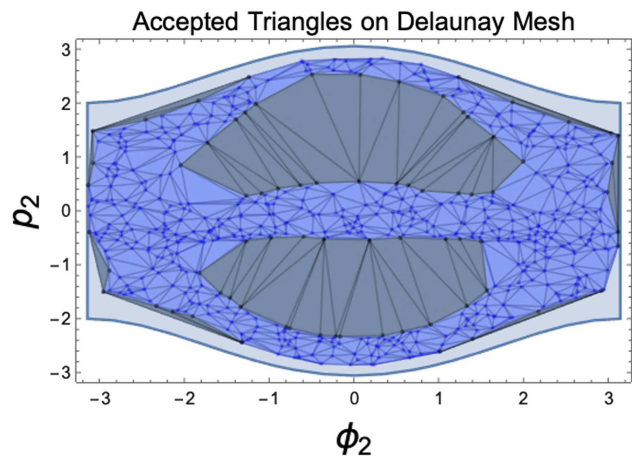


FIG. 15. Accepted (chaotic, shaded lighter/blue) and rejected (regular, shaded darker/gray) triangles on the Delaunay Mesh for a sample chaotic region on the “ $\varphi_1 = 0$ ” Poincaré surface at $E = 7$ for maximal edge length $d = 1$. The light colored region on the periphery inside the Hill region consists of regular sections.

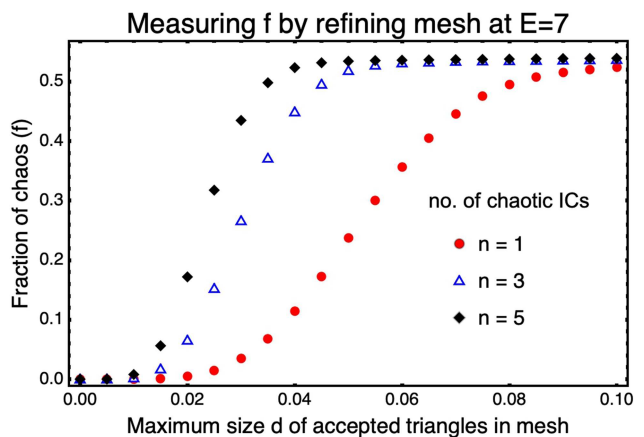


FIG. 16. Estimates of the fraction of chaos (area of accepted region/area of the Hill region) for various choices of d . An optimal estimate for f is obtained by picking d where f saturates. The three data sets displayed have $n = 1, 3, 5$ chaotic ICs, each evolved for the same duration $t = 10^5$.

area initially grows rapidly with d and then saturates for a range of d . Our best estimate for the area of the chaotic region is obtained by picking d in this range. Increasing d beyond this admits triangles that are outside the chaotic region. Increasing the number of points in the scatterplot (either by evolving each IC for a longer time or by including more chaotic ICs, which is computationally more efficient) reduces errors and decreases the threshold value of d as illustrated in Fig. 16.

REFERENCES

- ¹S. L. Sondhi, S. M. Girvin, J. P. Carini, and D. Shahar, "Continuous quantum phase transitions," *Rev. Mod. Phys.* **69**(1), 315 (1997).
- ²G. S. Krishnaswami and H. Senapati, "Stability and chaos in the classical three rotor problem," *Indian Acad. Sci. Conf. Ser.* **2**(1), 139–143 (2019).
- ³M. C. Gutzwiller, *Chaos in Classical and Quantum Mechanics* (Springer-Verlag, New York, 1990).
- ⁴J. Milnor, *Morse Theory* (Princeton University Press, NJ, 1969).
- ⁵H. Yoshida, "A type of second order ordinary differential equations with periodic coefficients for which the characteristic exponents have exact expressions," *Celest. Mech.* **32**, 73–86 (1984).
- ⁶M. Brack, M. Mehta, and K. Tanaka, "Occurrence of periodic Lamé functions at bifurcations in chaotic Hamiltonian systems," *J. Phys. A Math. Gen.* **34**, 8199 (2001).
- ⁷J. Hadjidemetriou, "Periodic orbits in gravitational systems," in *Chaotic Worlds: From Order to Disorder in Gravitational N-Body Dynamical Systems, Proceedings of the Advanced Study Institute*, edited by B. A. Steves, A. J. Maciejewski, and M. Hendry (Springer, 2006), pp. 43–79.
- ⁸R. C. Churchill, G. Pecelli, and D. L. Rod, "Stability transitions for periodic orbits in Hamiltonian systems," *Arch. Rational Mech. Anal.* **73**(4), 313–347 (1980).
- ⁹C. Lanczos, *The Variational Principles of Mechanics*, 4th ed. (Dover, New York, 1970), p. 139.
- ¹⁰G. S. Krishnaswami and H. Senapati, "Curvature and geodesic instabilities in a geometrical approach to the planar three-body problem," *J. Math. Phys.* **57**, 102901 (2016).
- ¹¹R. Montgomery, "N-body choreographies," *Scholarpedia* **5**(11), 10666 (2010).
- ¹²C. Moore, "Braids in classical gravity," *Phys. Rev. Lett.* **70**, 3675–3679 (1993).
- ¹³A. Chenciner and R. Montgomery, "A remarkable periodic solution of the three-body problem in the case of equal masses," *Ann. Math. Second Ser.* **152**(3), 881–901 (2000).
- ¹⁴S. L. Ziglin, "Branching of solutions and nonexistence of first integrals in Hamiltonian mechanics. I," *Funct. Anal. Appl.* **16**(3), 181–189 (1982).
- ¹⁵V. K. Melnikov, "On the stability of the center for time periodic perturbations," *Tr. Mosk. Mat. Obs.* **12**, 3–52 (1963) [Trans. Moscow Math. Soc. **12**, 1–56 (1963)].
- ¹⁶A. Lakshminarayan, M. S. Santhanam, and V. B. Sheorey, "Local scaling in homogeneous Hamiltonian systems," *Phys. Rev. Lett.* **76**, 396 (1996).
- ¹⁷B. V. Chirikov, "Resonance processes in magnetic traps," *At. Energy* **6**, 630 (1959) [*J. Nucl. Energy Part C Plasma Phys.* **1**, 253 (1960)].
- ¹⁸J. M. Greene, "Method for determining a stochastic transition," *J. Math. Phys.* **20**, 1183 (1979).